System Performance of an Over-Water Propagation for an LMDS Link

By
Chin Khee Tan

Thesis submitted to the Faculty of the
Virginia Polytechnic Institute and State University
in partial fulfillment of the requirements for the degree of

Master of Science
in
Electrical Engineering

Charles W. Bostian, Chair
Timothy M. Pratt
Dennis G. Sweeney

April 17, 2001
Blacksburg, VA

Keywords: LMDS, Reflection, Scattering, Bandwidth, Data Rate, Bit Error Rate, Simulation

System Performance of an Over-Water Propagation for an LMDS Link

Chin Khee Tan

ABSTRACT

The growth of broadband Internet access has paved the way for the development of many newer existing technologies. As the costs of implementing broadband access soar, the best alternative will be to use wireless technologies. At a carrier frequency of about 28 GHz, the potential benefits of Local Multipoint Distribution Service (LMDS) will eventually outweigh those of its current competitors in the wired market. Since the rural communities will reap the most benefits from this technology due to its low costs, studies on the channel behavior and terrain relationships must be done.

This thesis aims to provide a preliminary study on the effects of propagating an LMDS signal over a lake surface. Currently, there is not enough information to prove the feasibility of deploying an LMDS system for this terrain. Some background on the technology and rough surface theory is provided for the reader to better understand the environment that is being investigated. Simulation results are presented as a guide to assist future researchers to conduct a field measurement campaign. A block diagram of a potential measurement system is also provided to aid in the development of the tools necessary for the measurement of an actual channel.

ACKNOWLEDGEMENTS

I will begin by thanking all my fellow comrades at the Center for Wireless Telecommunications (CWT) for the endless help and support that I have been endowed with. Having the opportunity to work with some of the wireless industry's greatest minds has been a privilege that I will continue to cherish.

I would like to extend my most sincere appreciation to my advisor, Dr. Charles Bostian, for paving the way for me to explore in the development of this thesis.

I owe a particular debt of gratitude to Dr. Dennis Sweeney, who provided me with his initial exploration of this research project. A fair amount of this thesis was written from his ideas, especially the setting up of a practical measurement campaign.

Dr. Timothy Pratt has been instrumental in guiding my through the simulation of digital systems, especially in filter designs and eye patterns.

The amount of knowledge that I gained from studying the surface roughness would not be possible without the assistance that I received from Dr. Gary Brown. In a field filled with uncertainties and unpredictability, without any doubt, I wouldn't have been as certain as I am about the ambiguity of rough surfaces.

I was fortunate enough to work with Carl Fossa, Max Robert, Wachira Chongburee, and Michael Lei who have assisted me with many of the digital communication theory designs.

Adelia Valdez has been a great inspiration for me in getting myself acquainted with MATLAB. A significant part of the source code was originally written by Ms. Valdez,

especially the filter designs and eye diagrams. The codes were modified to suit this particular simulation.

Last but not least, I am eternally grateful to my family, for without their love and support, I wouldn't have the opportunity to pen down these words.

CONTENTS

List of Tables

List of Figures

Chapter 1

Introduction

1.1 Introduction to the LMDS Technology

Local Multipoint Distribution Service, more commonly known as LMDS, is one of the most effective and inexpensive way to solve the 'last-mile' bottleneck problem that has plagued Internet users all over the world. Traditional telephone lines that connect to most existing structures have been around since the middle of the 20th century. They were originally designed to handle low capacity and low data rate voice traffic. Since the introduction of the Internet in the last decade, the increasing need for wider bandwidths and capacity seems to outgrow the limited capacity of the copper wires that connect to our homes.

Although switching centers are connected to the Internet via high-speed fiber optic backbones, not all users at home and at the office are able to enjoy the luxury of having high-speed connections. A T-1 (1.544 Mbps) connection can cost up to $1500 per month. With this in mind, researchers are struggling to solve this problem and to provide short-range, broadband access to all end-users. The most obvious solution to this problem need not come from the laying of new infrastructure in the ground, but to use a high-frequency wireless carrier, thus spawning the technology that is LMDS.

There are three types of LMDS connections available so far. The simplest configuration is a point-to-point (P2P) connection, where the communication link is between one hub and one Customer Premise Equipment (CPE). The Point-to-Multipoint (PMP) configuration, where each base station serves several CPEs at the same time, is the more commonly used system, as most equipment manufacturers are using Time Division Duplexing (TDD) with Time Division Multiple Access (TDMA) to promise an increase in capacity. A new technology that surfaced, recently typified by Radiant Networks PLC, introduced the mesh configuration. It defies the traditional hub–terminal communication link by allowing each node to be interconnected using multiple integrated P2P links. In other words, any node in the cell can act as the hub [Rad00].

LMDS antennas need not be large due to the short wavelengths of the high-frequency carriers. This allows the façade of most buildings that maintain an LMDS antenna to be aesthetically pleasing.

In the United States, the LMDS frequency spectrum has two components. The first, known as the A Block, spans from 27.5 to 28.35 GHz, 29.10 to 29.25 GHz, and 31.075 to 31.225 GHz. The B Block covers the spectrum from 31.000 to 31.075 GHz and 31.225 to 31.300 GHz. Total available bandwidth allocated by the Federal Communications Commission (FCC) is 1300 MHz. The A Block has the highest amount of RF bandwidth, at 1150 MHz. This bandwidth is higher than all of the other bandwidths used by lower frequency services combined.

Since most deployed LMDS systems are still in their beta phase, studies are still being conducted to improve the quality of service (QoS) of this system. One major problem that continues to affect LMDS systems is wavelength. At 28 GHz, the wavelength of the carrier is only about 1 cm. At this wavelength, the system is very susceptible to the environment. A line-of-sight (LOS) has to be available from the transmitter to the receiver. Reflection and scattering of the waves will affect the quality of the transmission if the waves do not have a first Fresnel zone clearance.

1.2 Motivation for Research

As Virginia Tech strives to provide broadband services to communities of southern parts of the state of Virginia, feasibility studies have to be conducted to ensure an acceptable quality of transmission.

One of the areas that is of increasing interest is Smith Mountain Lake in Southwestern Virginia. The difference between this area and others is that the propagation of the radio waves has to be transmitted over water. For LMDS wavelengths, the calmest of water surfaces seems rough. The motivation for this research is to study the effects on the bandwidth as the signals propagate over water.

In [Nar96], a technique was developed to separate the specular and diffuse components of a reflected signal. In their paper, the authors studied various terrains including lake surfaces, while changing the height of the antennas. In this thesis, the antenna heights will remain constant, while only the level of the lake will change in the course of the day. The emphasis of this research is on the performance of digital signal transmission over the water surface.

Chapter 2 provides the reader with some background information on millimeter wave characteristics, and some basic propagation theories, including free space propagation, reflection, and scattering. Chapter 3 describes the modeling of the Smith Mountain Lake terrain and provides the essential parameters that are being used in the simulation process.

The simulation results are shown in Chapter 4. Chapter 5 describes how the results affect a potential LMDS communication link. Suggestions as to how to conduct a field measurement campaign will be outlined and a block diagram of a possible hardware configuration will be provided. The remaining questions that will be answered are what has to be measured and how it will be measured.

Chapter 2

Background and Theory

Since this research thesis is based on propagating LMDS signals over water, specifically Smith Mountain Lake, we will begin by providing some background about the terrain.

Many of the existing propagation models, much like the one described in [Par94], would not work with the odd geometry of Smith Mountain Lake and the type of communication link that will be used. Instead of a path that varies in distance and in the height of the transmitter and the receiver, the lake surface height changes throughout the day depending on the need for hydroelectric power in the region, while the transmitter and receiver are fixed in location.

The variation of the lake level is the key motivation for this research. All non-mobile links use fixed transmitter and receiver locations. Current propagation models developed in countless literatures deal mostly with the mobile environment, while not much emphasis has been put into broadband fixed wireless communications until recently.

At such a high operating frequency, namely at 28 GHz, the calmest of water is rough due to the short wavelength of about 1 cm. This causes diffused scattering of the reflected signal from the water surface to the receiver.

2.1 History of Smith Mountain Lake

Smith Mountain is in the southwestern Virginia counties of Pittsylvania and Bedford, where the Smith Mountain Lake/Dam is located. The precise location can be seen in Figure 2.1. It was built and operated by the Appalachian Power Company, now known as the American Electric Power Company (AEP). This dam is part of a pumped storage and hydroelectric development project from the 1960s to generate electricity during times of peak demand by customers in the region. Leesville Dam in Campbell and Pittsylvania counties is also a part of this development initiative [Roa01].

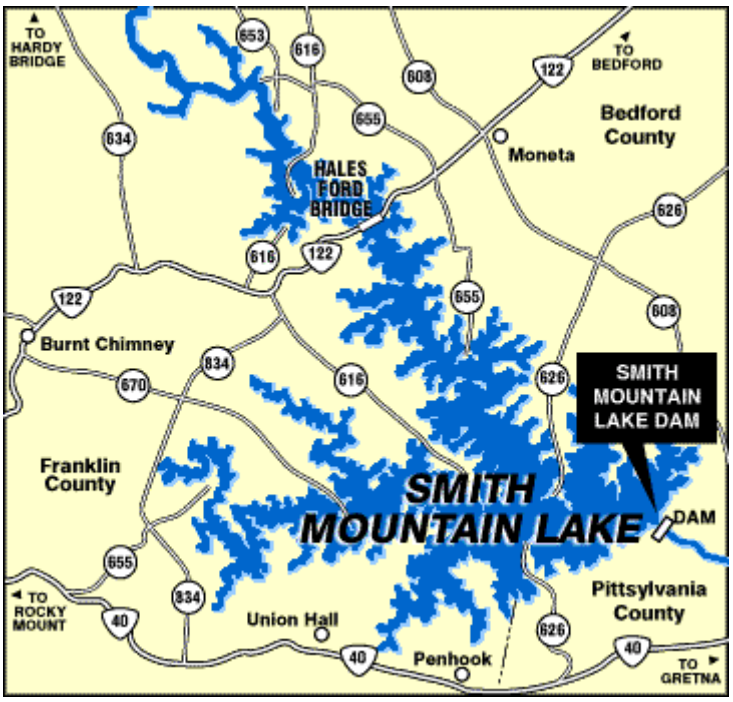

Figure 2.1: Location of Smith Mountain Lake [Roa01]

The generation of electricity in the Leesville/Smith Mountain Dam takes place primarily during times of peak demand, which occurs during the weekdays. In the evenings, nights, weekends, and holidays, when demand is low, the water is pumped back into the upper lake (Smith Mountain Lake), causing the water level to rise. Water is pumped into the lower lake (Leesville Lake) when demand is high, causing the water level to fall. The dam is shown in Figure 2.2.

Figure 2.2: Smith Mountain Lake / Dam [Roa01]

In order to provide broadband Internet access to the communities around the Smith Mountain Lake, its terrain has to be studied so that an effective and efficient network can be built in the region. The interesting problem that lies in this terrain is the lake itself. The issue is not getting the radio waves to propagate over the lake, but rather getting acceptable performance from an over-water path. Although countless research has been done on over-water propagation, the studies were mainly concentrated on narrow bandwidths at lower frequencies over an open water surface like the ocean or the sea. This thesis attempts to study a much wider bandwidth operating at high frequencies for the purpose of deploying an LMDS system in the region.

2.2 Characteristics of Millimeter Waves

There has been a heightened interest in developing communication systems at higher frequency ranges. The problem of congestion in the lower frequency spectrum contributes to the advancement of research technology to develop communication equipments at higher frequencies. This need is the main motivation behind the development of broadband access technologies, the key to LMDS systems.

Optical fiber communications, although more reliable and offering more bandwidth, are expensive to implement. The cost of laying fiber optic cables from the switching centers to homes or office buildings is tremendously high. This is another key reason for researchers to create new alternatives like LMDS and other related services. The idea is to provide a last-mile solution from the switching center to the home or office. In other words, it is mainly for short range, high frequency transmission systems.

One other advantage of employing millimeter wave communication links is that the antennas need not be large. This is especially important for owners and occupants of large office and home structures to maintain an aesthetically pleasing façade.

The wireless broadband industry is still, at the time this thesis is being developed, fairly new. There are no proven cases where it is being successfully deployed and being used by a majority of the population. Cases of deployment are exclusively for university research or communication links between office campuses.

The interesting idea of using millimeter waves for communication because of its large available spectrum poses many problems for researchers. One of the main problems is the need for a line-of-sight (LOS) between the transmitting and receiving antenna.

At millimeter wavelengths, there is little or no diffraction around buildings and terrain features; trees and other vegetation will absorb the signals. Rain drops and snow will also absorb and scatter these signals, further degrading the quality of service of LMDS systems. At times of heavy rain and thunderstorms, the receiver may not be able to receive any signals.

2.3 Theory of Radio Wave Propagation

The figure below illustrates the basic idea of a simple microwave radio link. An essential part of systems engineering in radio communications is the determination of the free space propagation path, illustrated by P_{dir}.

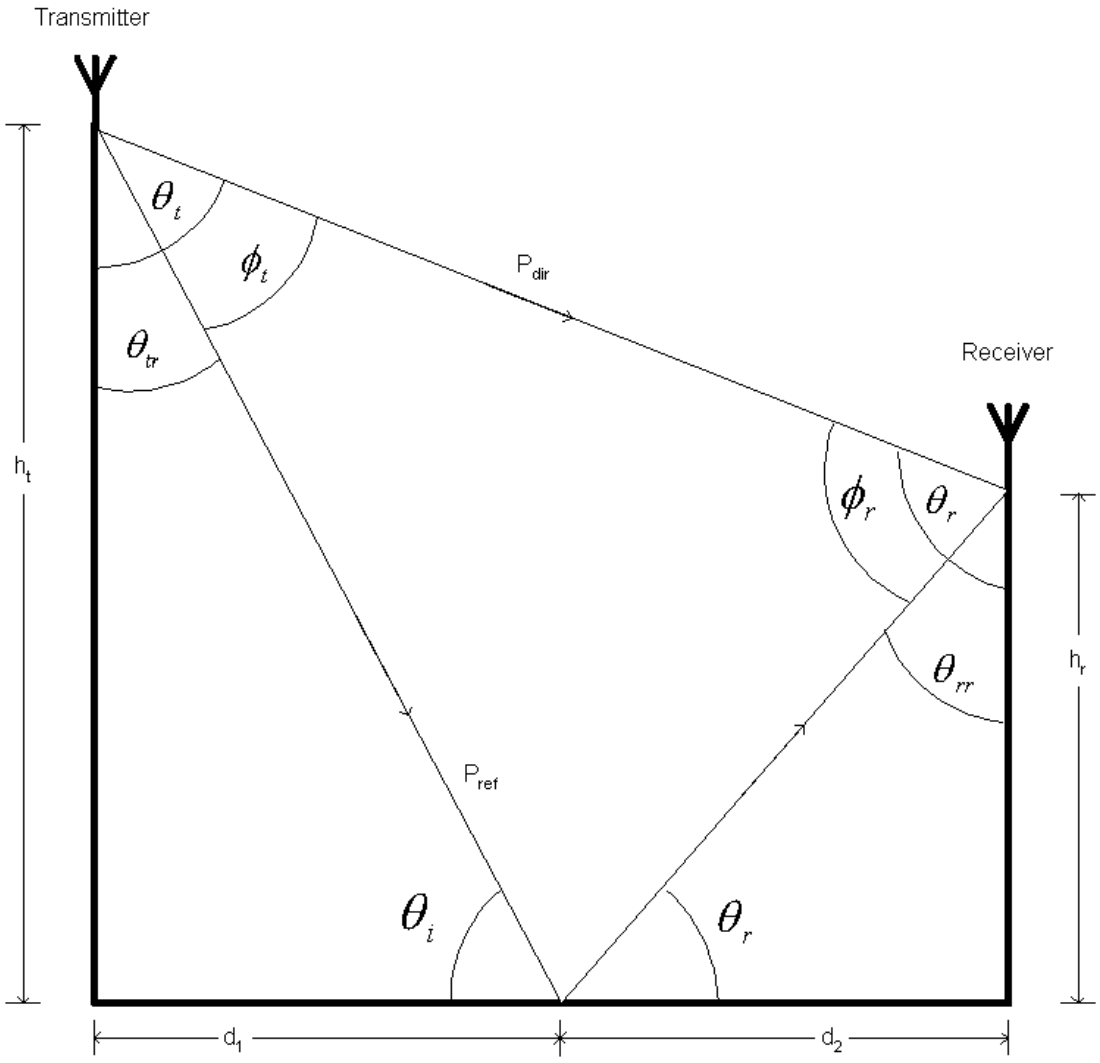

Figure 2.3: Transmission paths between the transmitting and receiving antennas

Additional paths, contributed by the surface reflections and atmospheric refractions, could damage or impair the received signal at the receiver. This is because waves moving

along the additional paths could either add constructively or interfere with the waves that arrive in the direct path. The fluctuation in signal levels resulting from the interference of these multiple signal paths is called multipath fading.

2.3.1 Free Space Propagation

Consider an isotropic transmitter and receiving antenna. The gain, G of an antenna is given by

$$G = \eta \frac{4\pi}{\lambda^2} A_e , \tag{2.1}$$

where A_e is the effective aperture of the antenna.

λ, described by

$$\lambda = \frac{c}{f_c}, \tag{2.2}$$

is the wavelength of the carrier wave, where f_c is the carrier frequency (Hz), c is the speed of light (m/s) and η is the ohmic efficiency of the antenna. In most cases, η is assumed to be unity (ideal).

In all radio communications, the received power depends directly on the distance between the transmitting and receiving antenna. In a fixed link system, it can be assumed that the received power in a free space model remains constant, and only changes with frequency. In this manner, the Friis free space equation, given by

$$P_r = \frac{P_t G_t G_r}{L} \left(\frac{\lambda}{4\pi d} \right)^2 , \tag{2.3}$$

where

$P_r \equiv$ Received power

$P_t \equiv$ Transmit power

$G_t \equiv$ Transmitting antenna gain

$G_r \equiv$ Receiving antenna gain

$d \equiv$ Distance between transmitter and receiver

$L \equiv$ System loss (not related to propagation) ,

can be used to estimate the received power of an antenna at a fixed distance. The second part of the equation, given as the squared component in parenthesis, is the inverse of the free space path loss component.

2.3.2 Reflection

Reflection occurs when a propagating electromagnetic wave impinges upon a surface which has very large dimensions when compared to the wavelength of the propagating wave [Rap99]. In Figure 2.3, the reflected path is illustrated by P_{ref}.

Due to the difference in the electrical properties between the two media (water and air) at which the wave is propagating, namely the permittivity (ε), permeability (μ), and conductivity (σ) of the medium, the wave could either be partially transmitted or partially reflected.

For different polarization techniques, ie. horizontal and vertical (as seen in Figures 2.4 and 2.5 respectively), the reflection coefficient of the ground differs with the different values of ε, μ, and σ. This causes both the amplitude and phase to change depending on these coefficients.

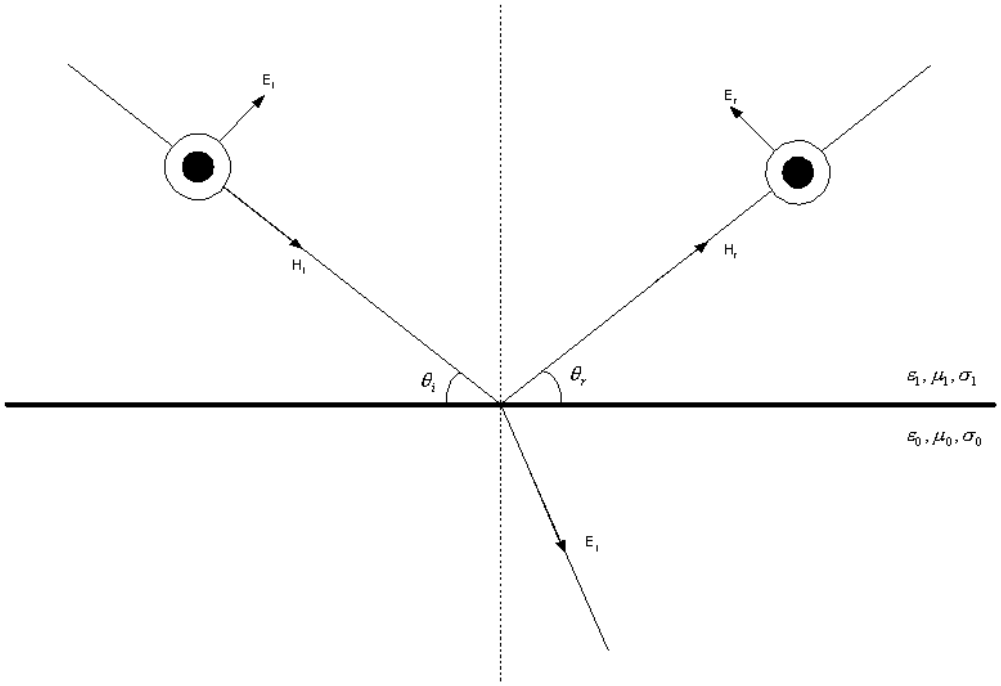

Figure 2.4: E-field in the plane of incidence. Horizontal polarization [Rap99].

As explained in [Par94], the reflection coefficient of a horizontally-polarized wave incident on the surface of the earth is:

$$\Gamma_h = \frac{E_r}{E_i} = \frac{\sin\theta - \sqrt{(\varepsilon - \varepsilon_0 - j\sigma/\varpi\varepsilon_0) - \cos^2\theta}}{\sin\theta + \sqrt{(\varepsilon - \varepsilon_0 - j\sigma/\varpi\varepsilon_0) - \cos^2\theta}} \quad , \tag{2.4}$$

where ε_0 is the dielectric constant of free space and ω is the angular frequency.

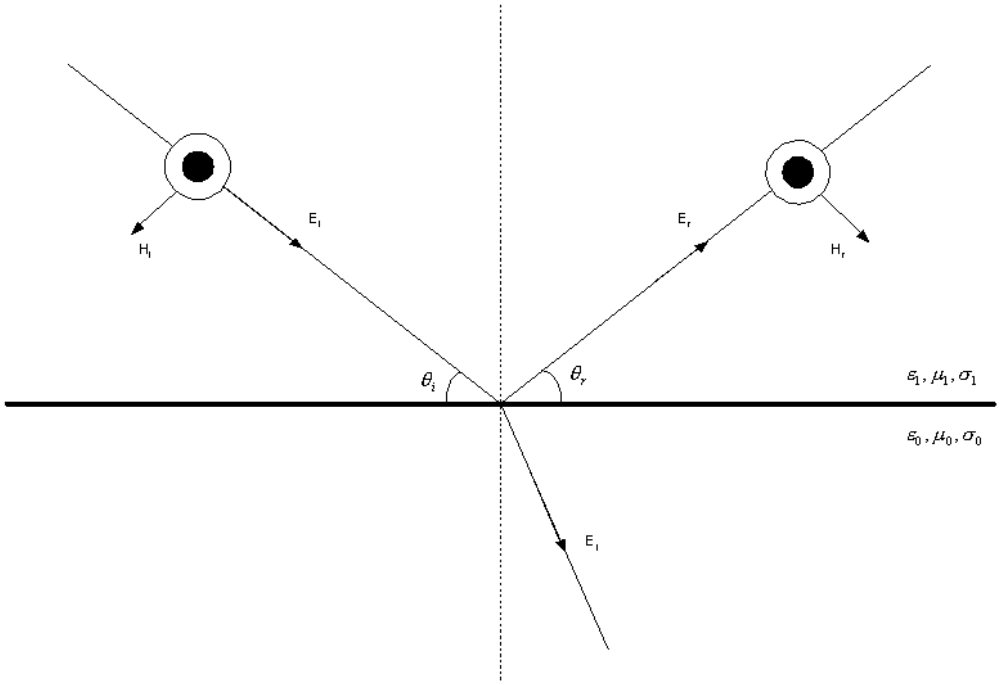

Figure 2.5: E-field normal to the plane of incidence. Vertical polarization [Rap99].

The reflection coefficient of a vertically-polarized wave, similarly, is given by

$$\Gamma_v = \frac{E_r}{E_i} = \frac{(\varepsilon_r - jx)\sin\theta - \sqrt{(\varepsilon_r - jx) - \cos^2\theta}}{(\varepsilon_r - jx)\sin\theta + \sqrt{(\varepsilon_r - jx) - \cos^2\theta}} \quad , \tag{2.5}$$

where

$$x = \frac{\sigma}{\omega\varepsilon_0} = \frac{18(10)^9\sigma}{f} \quad .$$

A careful observation of both Equations 2.4 and 2.5 reveals that the components are complex. This causes the magnitude and phase of the reflected wave to differ from the incident wave.

2.3.3 Surface Roughness and Scattering

Previously, the discussion on reflection assumes strictly that the surface of reflection was smooth, and therefore, only specular reflection takes place. However, when the surface is rough, the smooth surface analysis will not be realistic. Diffuse reflection occurs to the reflected wave; this situation is better known as scattering. Since only a small fraction of the scattered waves is directed to the receiving antenna, a whole new analysis has to be done to observe the random nature of the surface. A single, complex reflection coefficient as given in the previous section will not be enough to quantify the effects. The following discussions will provide the reader with a better understanding of what constitutes a rough surface.

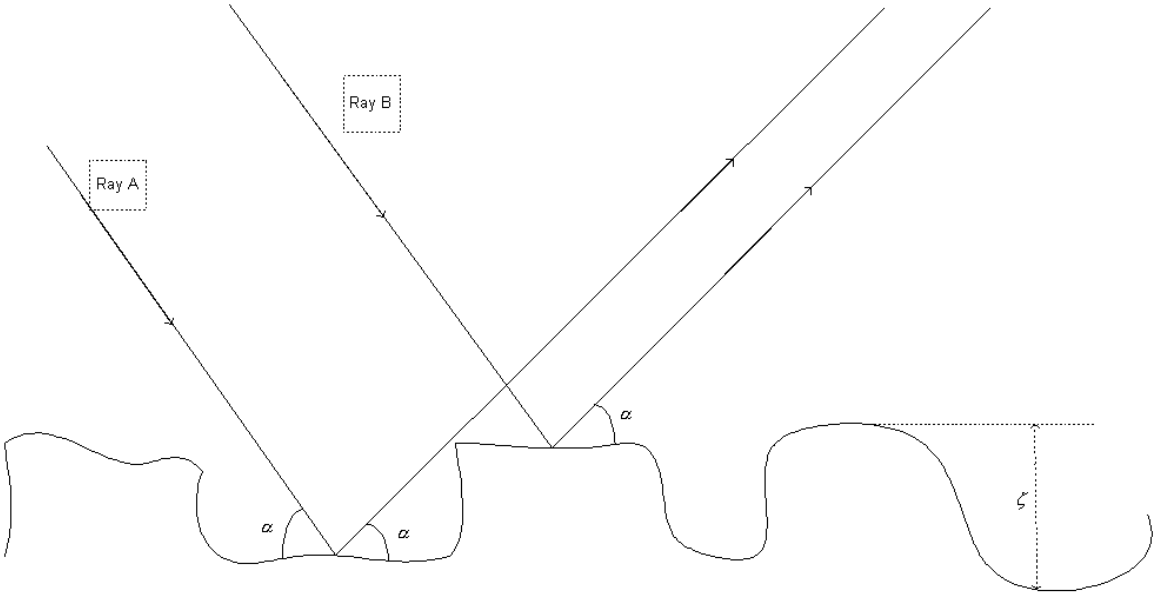

Figure 2.6: Illustration of two ray scattered from a rough surface. This is an idealized model for rough surface scattering.

Both rays of Figure 2.6, A and B, are incident on a surface with irregularities of height ς at a grazing angle α. The path difference between the two rays is

$$\Delta d = 2\varsigma \sin(\alpha) \tag{2.6}$$

with a phase difference of

$$\Delta\varphi = \frac{4\pi\varsigma}{\lambda}\sin(\alpha). \tag{2.7}$$

From both of these equations, it is possible to realize that when the phase difference is π rad, both rays will be in opposing phases and will thus cancel in phase. In a similar manner, when the phase difference is 0 or 2π rad, the two rays will add in phase. The Rayleigh criterion, a rule of thumb that is used in many remote sensing techniques, states that

$$\varsigma \leq \frac{\lambda}{8\sin(\alpha)}. \tag{2.8}$$

A closer look at Equation 2.8 tells us that since the wavelength of millimeter waves is small, most surfaces can be assumed to be rough.

2.3.4 Diffuse Scattering

We have explained that specular reflection is caused by a smooth surface. The reflected signal's phase is coherent and reflected power is directional, thus obeying the laws of classical optics [Bec63].

Diffuse scattering, on the other hand, has very little directivity and usually takes place over a much larger surface area than specular reflection. Its phase is incoherent, thus there may be large fluctuations in amplitude. This is illustrated in Figure 2.7.

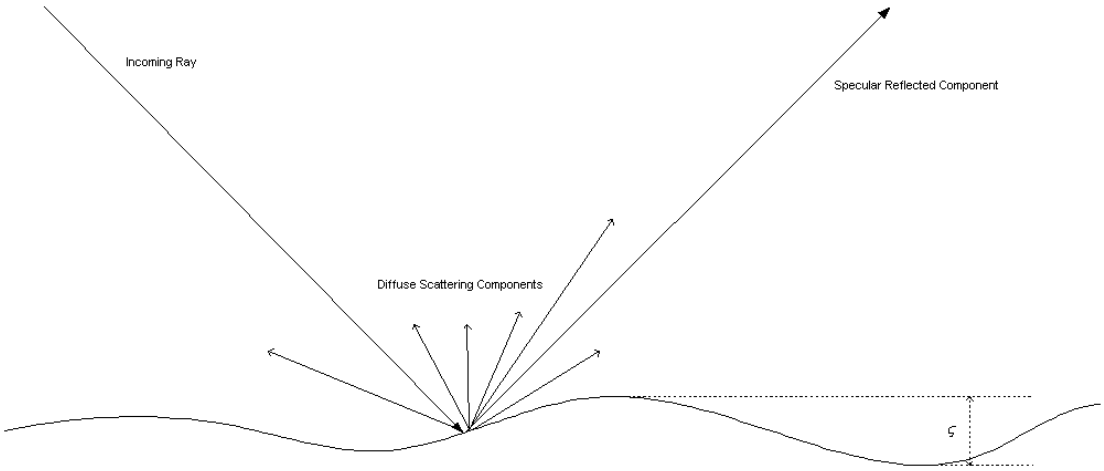

Figure 2.7: Illustration of Specular and Diffuse Scattering

This is a more practical model to describe the surface of the earth, compared to Figure 2.6. The illustrated surface irregularity represents a more realistic earth surface.

We will now introduce a variable, $<\varsigma^2>$, as the mean square roughness of the surface at which the incoming wave is being scattered and reflected.

The Rayleigh criterion can now be expressed as

$$C = \frac{4\pi\sigma \sin\alpha}{\lambda} \quad , \tag{2.9}$$

where σ is the standard deviation of the surface irregularities relative to the mean height.

For C < 0.1, the surface can be considered smooth, and specular reflection can be assumed. When C > 10, highly diffuse reflection occurs and the reflected wave can be neglected altogether [Par94].

2.3.5 Coherent and Incoherent Power for the Reflected Wave

The wave number, given by k_0, is

$$k_0 = \frac{2\pi}{\lambda} \quad . \tag{2.10}$$

The coherent power of the scattered signal depends on both the angle of reflection and the mean square roughness of the surface, while the incoherent power depends entirely on the mean square surface roughness.

In [Gee90], Brown derived the theory behind the relationship between the coherent and incoherent power distribution. The incoherent power can be thought of as noise, since it is scattered power from all directions combined and does not have a clear path. As the incoherent power dominates the profile, the coherent power will decrease to compensate for it.

The following figure illustrates the relationship between the coherent and incoherent power distribution. Its application with respect to this thesis will be explained in further detail in Chapter 5.

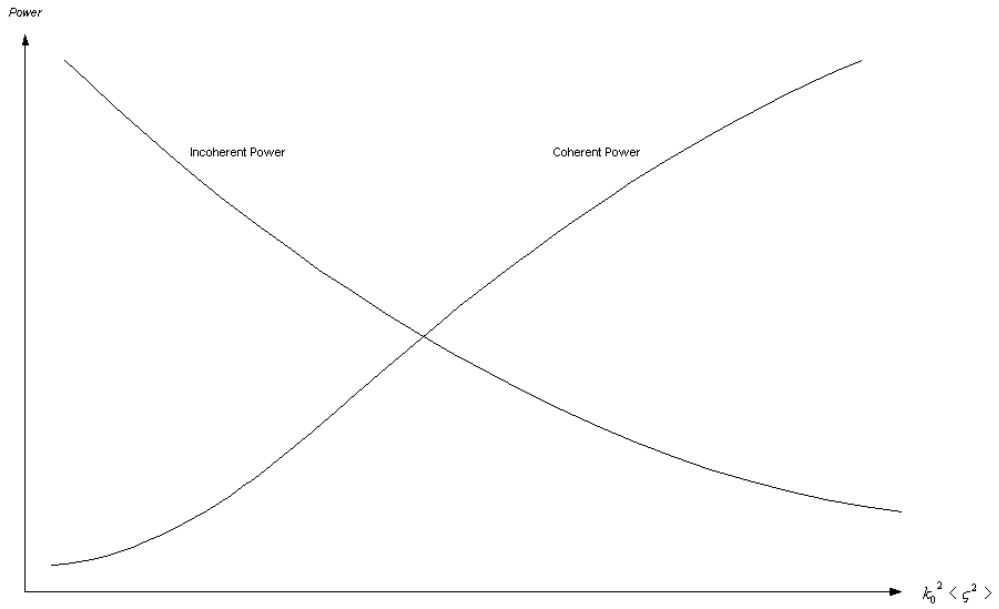

Figure 2.8: The relationship between the coherent and incoherent power distribution

The coherent power is proportional to

$$\exp\left(-4k_0^{\,2}\left\langle \varsigma^2 \right\rangle \sin^{-2}\alpha\right),$$

while the incoherent power is proportional to

$$\frac{1}{\left\langle (\nabla \varsigma^2)\ \right\rangle}\ .$$

The information provided will be sufficient to guide the reader through subsequent chapters of this thesis. Readers who are interested in learning more about the details of scattering and reflection are encouraged to consult the classic literature of [Bec63].

Oceanographers, throughout the years, have been trying to develop a specific model for all types of rough surfaces. Unfortunately, due to the unpredictable nature of water surfaces, there is no clear definition on how much the environment will affect the surface.

To illustrate this point, lake surfaces do not behave like the open sea surface. The slightest wind can cause the sea to have tremendously high waves. Based on the behavior of the incoherent power, one can assume for now that as the slope of the water surface becomes larger, the area in which the reflected wave will scatter becomes larger. As it grows, the amount of scattered power becomes dominant, and since it does not have any phase or directivity, it behaves very much like noise in a communication system.

Chapter 3
Methodology

3.1 Modeling the Smith Mountain Lake Terrain with a Modified Two-Ray Model

At this point, after going through the fundamentals of propagation, it is time to develop a propagation model for the Smith Mountain Lake terrain. We will start with the basic two-ray model. The idea of the two-ray model is to basically add the wave that is propagating in free space with the reflected component. A modified version of the model has to be made to suit the requirements of the terrain of interest.

In the Smith Mountain Lake terrain that we are investigating, the height of the transmitter far exceeds that of the receiver. This is one of the reasons that a modified propagation model needs to be derived. The two-ray model that is normally used assumes a distance d that is very large compared to the product of the height of the two transmitters divided by the wavelength. This model does not satisfy that requirement, which prompts us to take a different approach, based on the same idea.

The figure below illustrates the model that will be used in the simulation process.

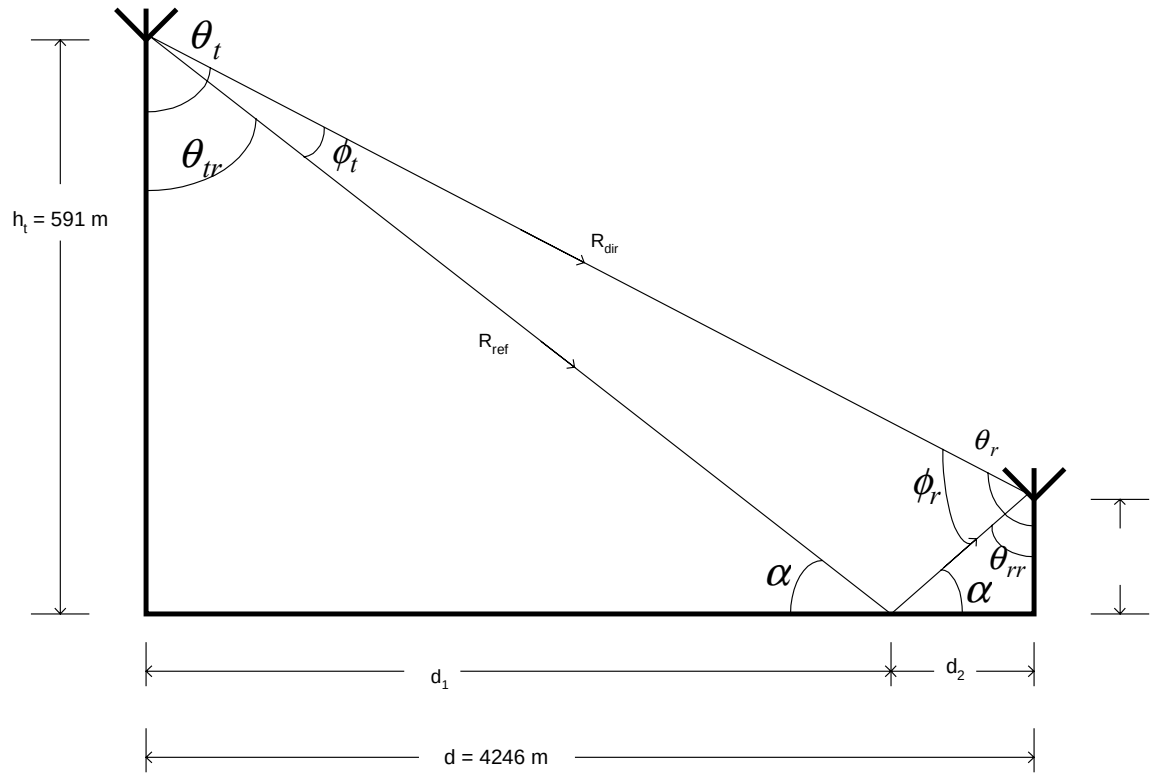

Figure 3.1: The Smith Mountain Lake two-ray model.

From Figure 3.1,

$$R_{dir} = \sqrt{d^2 + (h_t + h_r)^2} \tag{3.1}$$

where

$$d = d_1 + d_2 \tag{3.2}$$

$$R_{ref} = \sqrt{d_1^{\,2} + h_t^{\,2}} + \sqrt{d_2^{\,2} + h_r^{\,2}} \ . \tag{3.3}$$

We know that

$$\theta_i = \theta_r \tag{3.4}$$

$$d_1 = d - d_2 \tag{3.5}$$

$$d_2 = d - d_1 \ . \tag{3.6}$$

Equation 3.4 is also known as Snell's Law, which states that the incident angle will equal the reflected angle.

A thorough look at the incident and reflected angle yields

$$\theta_i = \theta_r = \alpha = \tan^{-1}\frac{h_t}{d_1} = \tan^{-1}\frac{h_r}{d_2} \quad . \tag{3.7}$$

Therefore,

$$\frac{h_t}{d_1} = \frac{h_r}{d_2} \quad . \tag{3.8}$$

Through algebraic manipulations, substituting Equation 3.8 into Equations 3.5 and 3.6 results in

$$d = \left(1 + \frac{h_t}{h_r}\right) d_2 = \left(1 + \frac{h_r}{h_t}\right) d_1 \ , \tag{3.9}$$

$$d_2 = \frac{d}{1 + \left(\frac{h_t}{h_r}\right)} \quad , \tag{3.10}$$

and

$$d_1 = \frac{d}{1 + \left(\frac{h_r}{h_t}\right)} \quad . \tag{3.11}$$

Substituting Equations 3.10 and 3.11 into Equation 3.3 results in

$$P_{ref} = \sqrt{{h_t}^2 + d^2\left(\frac{h_t}{h_r + h_t}\right)^2} + \sqrt{{h_r}^2 + d^2\left(\frac{h_r}{h_r + h_t}\right)^2} \quad . \tag{3.12}$$

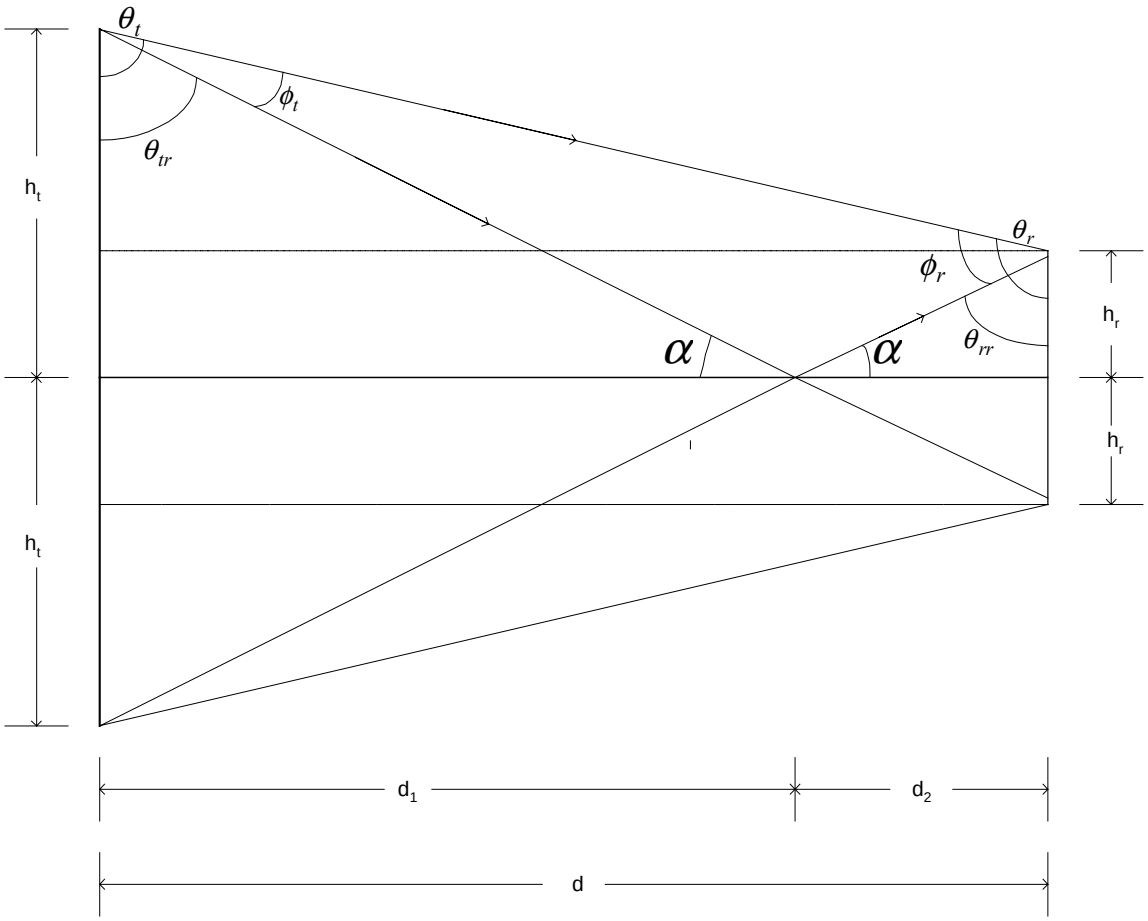

Figure 3.2: Using the method of images to illustrate the paths and angles of both the direct and reflected wave

From Figure 3.2, the following equations could be derived:

$$\theta_t = \tan^{-1}\frac{d}{h_t - h_r} \quad , \tag{3.15}$$

$$\theta_{tr} = \tan^{-1}\frac{d_1}{h_t} = \frac{d}{h_t + h_r} \quad , \tag{3.16}$$

and

$$\phi_t = \theta_t - \theta_{tr} \quad . \tag{3.17}$$

Similarly,

$$\theta_r = \tan^{-1}\frac{h_t - h_r}{d} \quad , \tag{3.18}$$

$$\theta_r = \theta_{rr} + 90^\circ \quad , \tag{3.19}$$

and

$$\theta_{rr} = \tan^{-1}\frac{d_2}{h_r} \quad . \tag{3.20}$$

We now introduce a variable that describes the path length difference between the direct and the reflected ray,

$$\Delta R = R_{dir} - R_{ref} \, . \tag{3.21}$$

The corresponding phase difference will be

$$\Delta\phi = \frac{2\pi}{\lambda}\Delta R \tag{3.22}$$

$$\Delta\phi = \frac{2\pi}{\lambda}\left[\sqrt{d^2 + (h_t - h_t)^2} - \sqrt{h_t^{\,2} + d^2\left(\frac{h_t}{h_r + h_t}\right)^2} - \sqrt{h_r^{\,2} + d^2\left(\frac{h_r}{h_r + h_t}\right)^2}\right] . \tag{3.23}$$

If the field strength at the receiving antenna due to the direct wave is E_d, the total received E-field is [Par94]

$$E = E_d\left[1 + \rho\exp(-j\Delta\phi)\right] \tag{3.24}$$

where ρ.exp(-jΔφ) represents the complex reflection coefficient.

$$= E_d\left[1 + \rho(\cos(\Delta\phi) - j\sin(\Delta\phi))\right] \tag{3.25}$$

By taking the absolute values,

$$|E|^2 = |E_d|^2\left[1 + \rho(\cos^2(\Delta\phi) - 2\cos(\Delta\phi) + \sin^2(\Delta\phi))\right]^{1/2} \tag{3.26}$$

$$= |E_d|^2\left\{1 + \rho\sin\frac{\Delta\phi}{2}\right\} . \tag{3.27}$$

Thus, power is proportional to the magnitude of the E-field squared.

A modified version of the Friis transmission formula, shown as Equation 2.3, where the path length difference is taken into account, is given as

$$P_r = 4P_t\left(\frac{\lambda}{4\pi d}\right)^2 G_t G_r \rho\sin^2\left(\frac{2\pi}{\lambda}\Delta R\right) . \tag{3.28}$$

Converting Equation 3.28 into decibels results in

$$P_r(dBm) = 6 + P(dBm)_t - 20\log_{10}\left(\frac{4\pi d}{\lambda}\right) + G_t(dB) + G_r(dB) + 20\log_{10}\left[\rho\sin\left(\frac{2\pi}{\lambda}\Delta R\right)\right] \tag{3.29}$$

Chapter 4

Simulation Results

The simulation was done with the model made to suit the terrain of Smith Mountain Lake as described in Chapter 3. The free space propagation results will be presented first, followed by the results obtained from a smooth reflection. A discussion on rough surface reflection would follow. The relationship between the carrier to noise ratio will then be presented, followed by the system performance with varying parameters.

A realistic approach was then applied to the system. A real digital system, modulated with the Quadrature Phase Shift Keying (QPSK) scheme was used in the simulation. The input signal was sent through the physical channel models with varying data rates, and the eye diagrams were plotted.

BER curves were generated for different lake levels and with varying data rate. These curves will show that as the data rate increases to a point where the Radio Frequency (RF) bandwidth of the signal exceeds the coherent bandwidth of the channel, the received signal will be degraded.

4.1 Free Space Propagation

From Figure 4.1 below, it is obvious that with only the direct path of propagation, the received power level will decrease as frequency increases because of the free space path loss component given in Equations 2.2 and 2.3. The transmitter power that was assumed in this simulation was 20 dBm, with a transmitter antenna gain of 20 dB, and a receiver antenna gain of 30 dB.

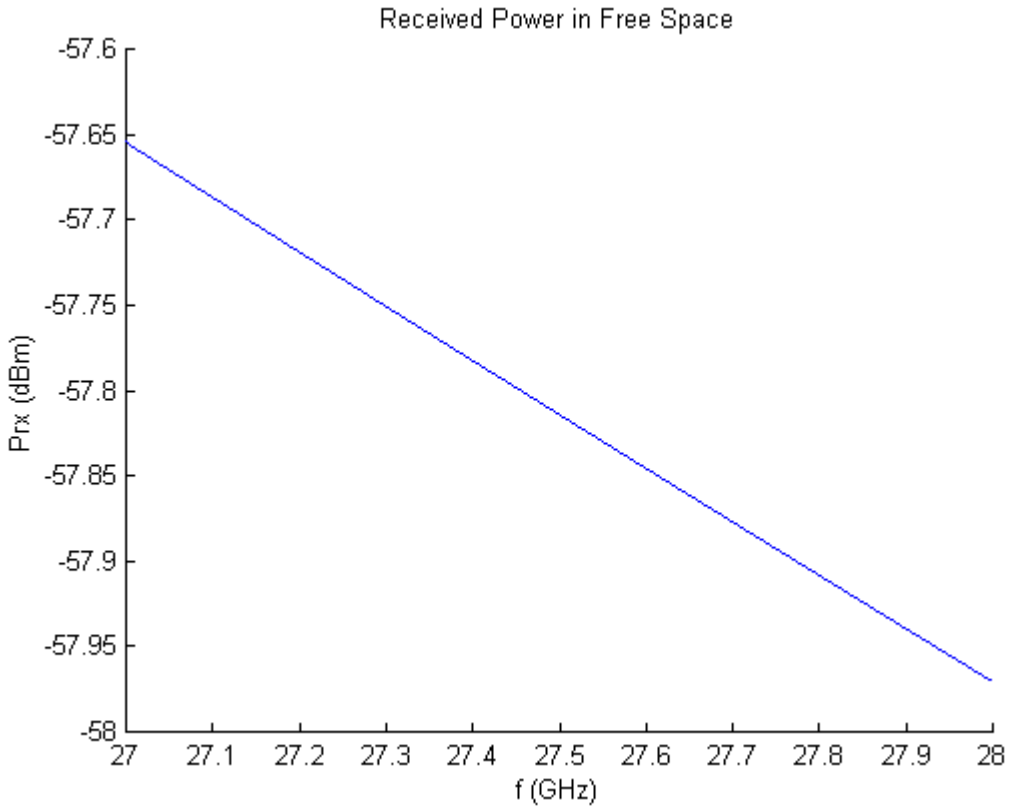

Figure 4.1: Received power in dBm plotted against frequency in GHz

4.2 Smooth Surface Reflection (Specular Reflection)

4.2.1 Received Power at Varying Lake Levels

The carrier frequency used in the simulation of Figure 4.2 was set at 27.5 GHz, and the lake level was made to vary from 239 m to 245 m with respect to the mean sea level. This observation is close to the actual situation at Smith Mountain Lake. At different times of the day, the water level is forced to rise and fall depending on the demand for hydroelectric power. The varying water depth has a direct impact on the observed result, caused by path length differences between the direct propagation path and the reflected path. This cycle repeats itself each time the difference in the path length is a half wavelength.

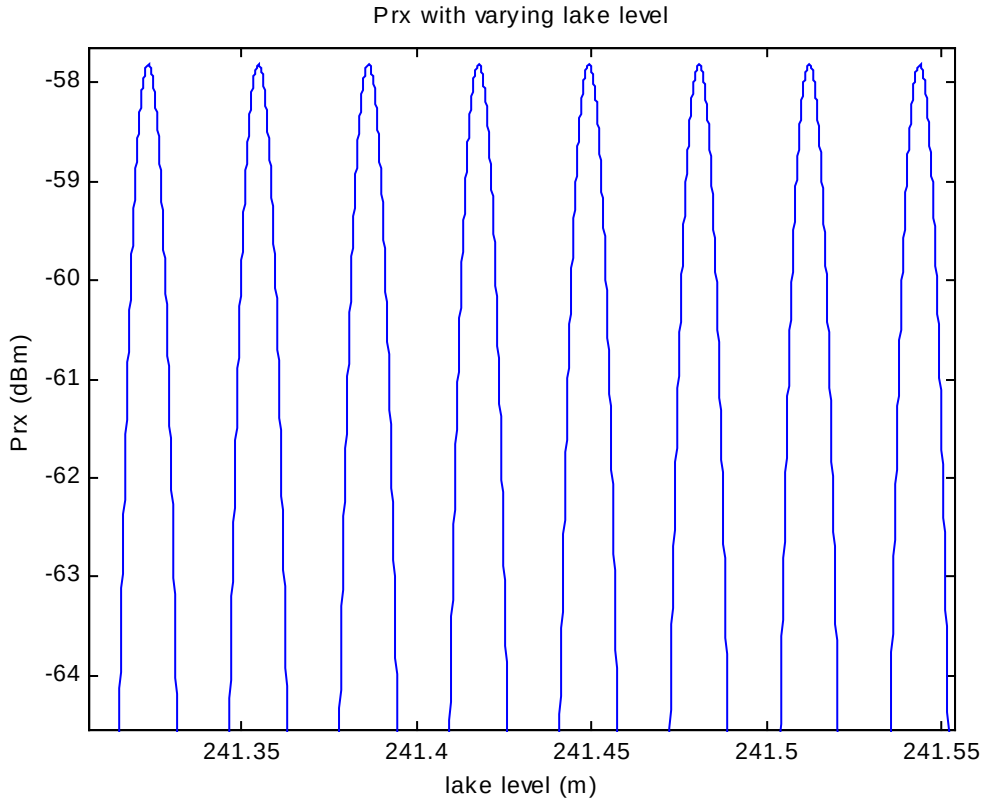

Figure 4.2: Received power in dBm varying with lake height. Carrier fixed at 27.5 GHz.

Normally, we would think of the received power variation as resulting from the movement of the transmitter and receiver heights. In this case, these parameters are fixed and the only component that changes is the lake level. This causes the path length difference, ΔR to change as well.

4.2.2 Power with Multipath Component

Setting the lake level at a specific height above the mean sea level allows us to perform a frequency sweep of the system to investigate the radio channel. At a certain time each day, the lake level will remain constant but data would still be transferred through the radio link. The fading effects could be observed by performing this simulation.

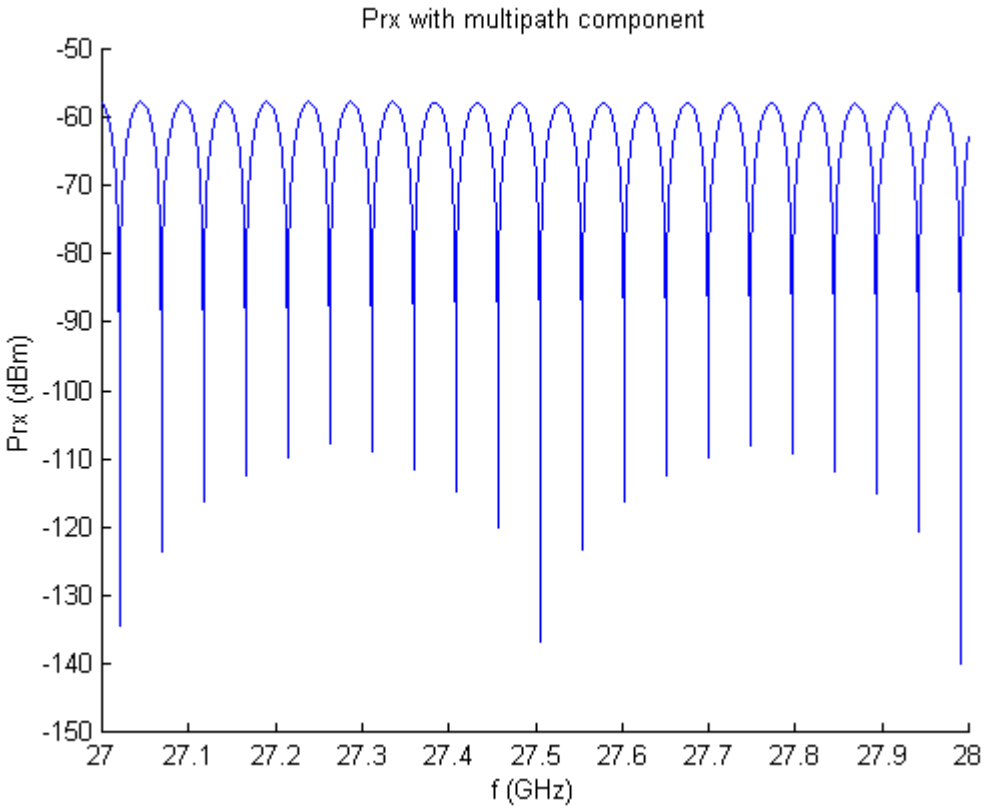

Figure 4.3 Received power with multipath.

Adding a multipath component reflected from the lake surface, as shown in Figure 4.3, distorts the received power significantly, creating nulls when the signals cancel. The observed nulls are due to the difference in the path length between the direct path and the reflected path. At every half wavelength of the system, the pattern repeats itself. When they add in phase, both rays will contribute to the higher overall received power. Similarly, when the two rays are out of phase, they cancel each other out, causing the nulls to occur.

It can be noted that the effective bandwidth of the system decreases as the reflected component becomes more significant. The plot below compares a system that has total reflection with one that has only a reflected wave with 20% of the power of the direct wave.

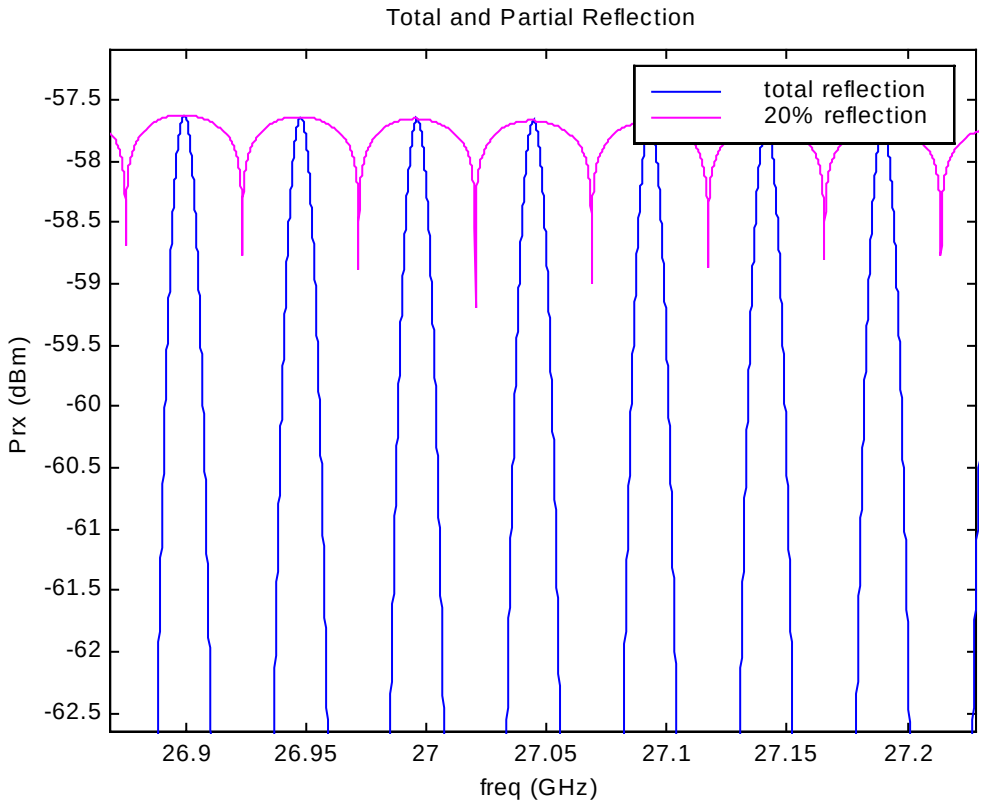

Figure 4.4: Received Power with total and partial reflection.

The figure above assumes two different reflection coefficients. Since the angle off boresite of the receiver antenna is large (refer φ_R in Figure 3.1), the receiver gain will decrease as the angle increases, if the same reflection coefficient were used for both waves, resulting in a plot similar to Figure 4.3.

4.3 Rough Surface Reflection

Signals that are scattered do not exhibit directivity or coherent phase. This causes the scatterers to distort the overall received power at the receiver. The electromagnetic waves that are scattered behaves very much like the little sparkles caused by wavelets in a pond on a sunny day. Most of the scattered components will contribute noise to the system, although some of the rays will contribute to the overall power if the phases happen to be coherent. A very crude but not very accurate way to include the effects of scattering is to use reflection coefficients that are less than unity. A simple sketch shown in Figure 4.6 shows us how the channel would look like.

There have been several studies on determining the effects of scattering in mobile radio propagation models. These models are simple two-dimensional problems that do not take into account the random distribution of the scattered signals. One such study was conducted by Kloch and Andersen [Klo97]. In the study, it was noted that

$$P_{diffuse} \propto \int_A \sigma_b dA \ , \tag{4.1}$$

where

$$\sigma_b \propto \rho \cos\theta_i \cos\theta_r \ , \tag{4.2}$$

and A is the area of the scattering surface.

In [Gee90, Chapter 10], Brown concluded that many of these models, although could provide some insights to the effects of scattering, do not have a realistically proven case. In light of this matter, this research will be focused entirely on the effects of total reflection of the waves, where the reflection coefficient is unity.

Figure 4.5 illustrates the received power as seen by the receiver when it is specularly reflected and when it is scattered.

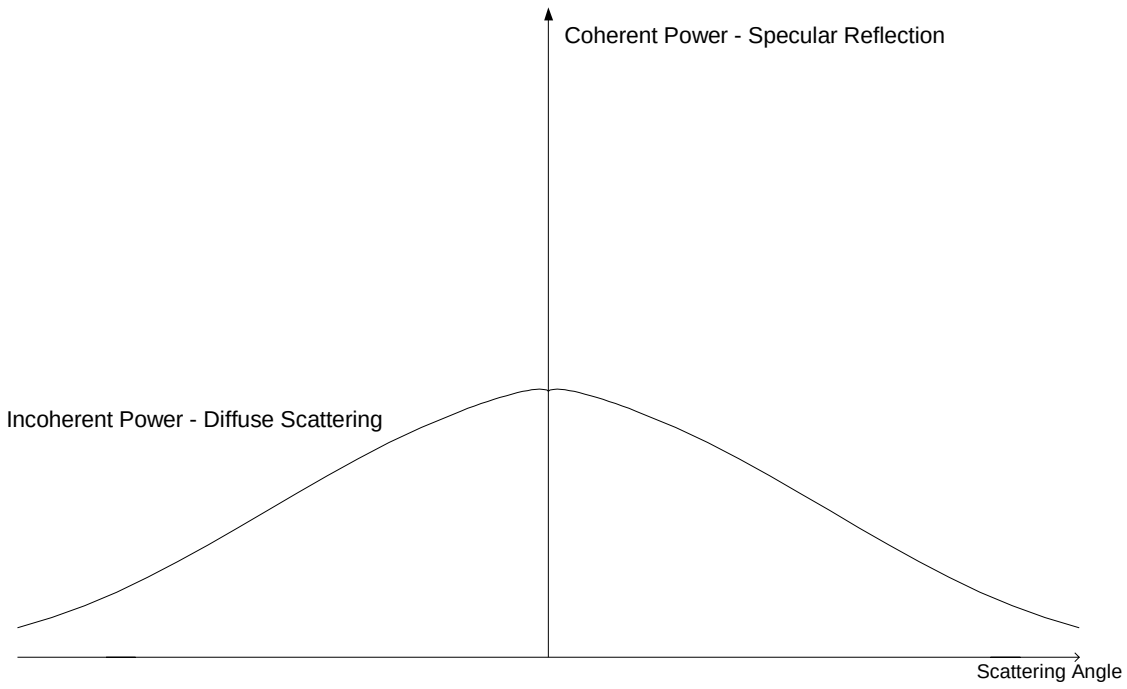

Figure 4.5: Illustration of coherent power and incoherent power

This sketch shows the magnitude of the reflected and scattered power as a function of the scattering angle for a wave that is normally incidence on the surface. As the angle deviation moves away from the incidence angle, the magnitude of the incoherent power decreases and spreads out farther.

This next figure shows how the received power is affected by the specularly reflected wave and if the reflected components were diffused.

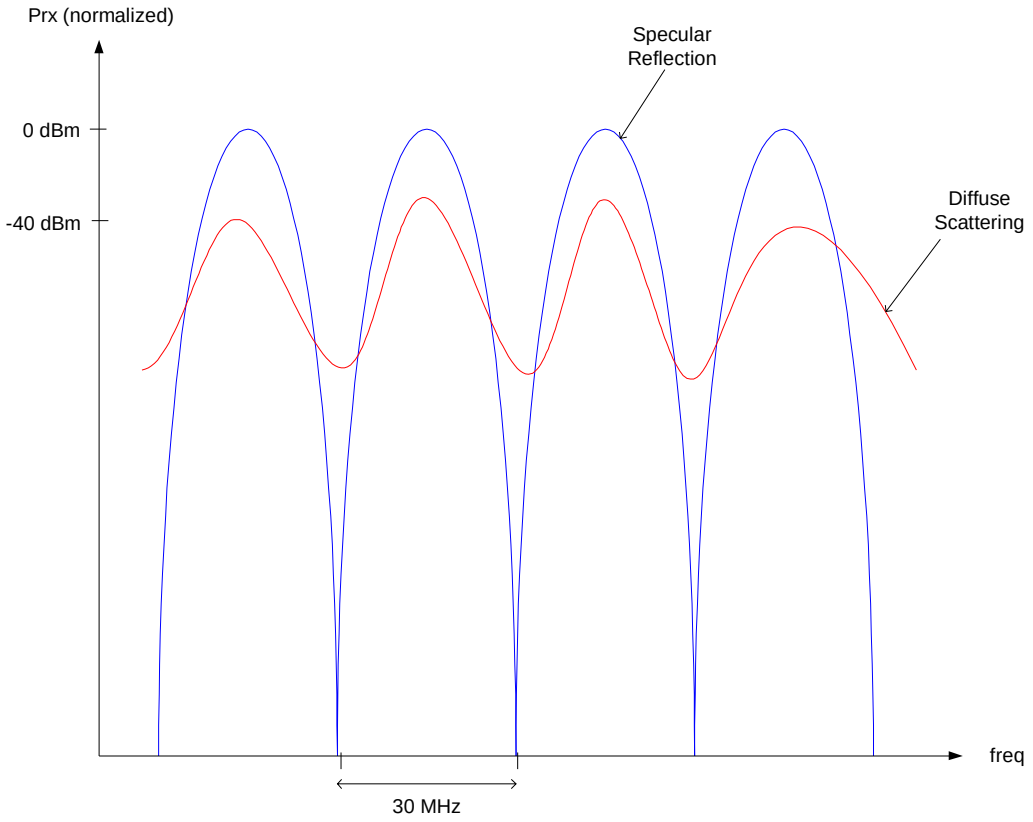

Figure 4.6: Illustration of received power with specular reflection and diffuse scattering

If the scattering effects are taken into account, the channel would behave as shown as the red line in Figure 4.6. The deep nulls that occur in total reflection will not be seen because some of the reflected waves are scattered and/or absorbed.

4.4 Bit Error Rate

In multi-layer modulation schemes such as 4-QAM (QPSK), 16-QAM, or 64-QAM, the bit error rate (BER) curve provides essential information on the performance of a communication link. The lower the BER requirements, the higher the C/N ratio has to be. If we observe the signal constellations, as the modulation indices increase, the symbols are closer to each other, thus increasing the probability of errors. This means that the C/N ratio will have to increase as the modulation index increases.

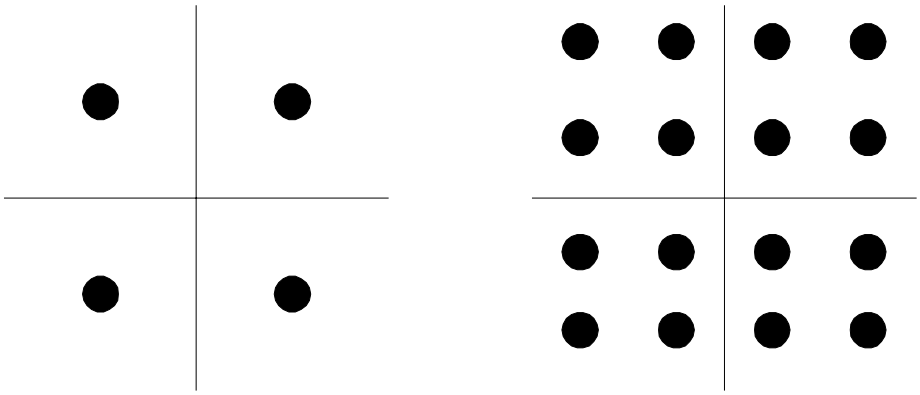

Figure 4.7: Signal constellation for 4-QAM (QPSK) and 16-QAM.

The BER curve can be generated by using the equation given as follows.

$$BER = \frac{4}{k}\left(1-\frac{1}{2^{k/2}}\right)Q\left(\sqrt{\frac{E_{d\min}}{2N_o}}\right) \tag{4.3}$$

where

$$E_{d\min} = \left(\frac{6k}{2^k-1}\right)E_b \ .$$

In practice, the carrier-to-noise ratio (C/N) is often used in place of the E_b/N_o. Their relationship is described below.

$$\frac{C}{N} = \frac{E_b}{N_o}\frac{R_b}{B} \tag{4.4}$$

Figure 4.8 below shows the BER vs C/N plot for three modulation types. As shown in the plots, an increase in the modulation index increases the C/N requirement for the same BER performance.

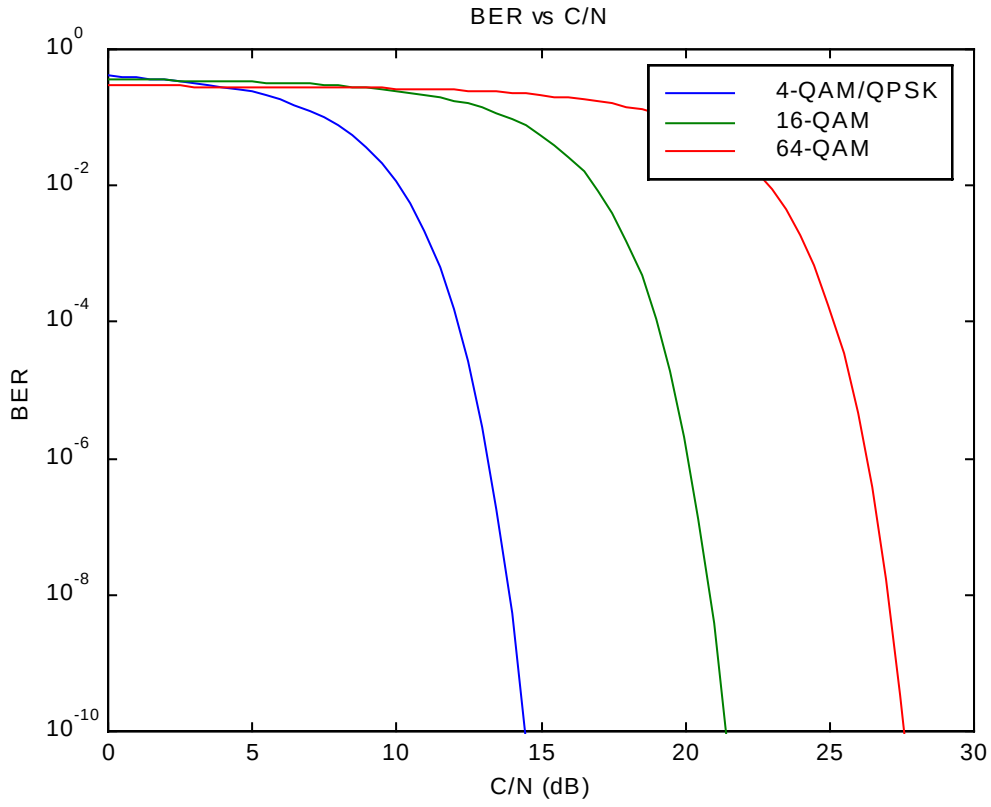

Figure 4.8: BER plotted against C/N.

We can see from the plot above, that for a system that is QPSK modulated, a C/N ratio of 13.6 dB is required to achieve the bit error rate performance of 10^{-6}.

4.5 Imperfect Channel

4.5.1 Channel Impulse Response

Figure 4.9 shows the impulse response of the channel in time. We can see that the direct free space path arrives at the receiver, followed by the reflected component with total reflection.

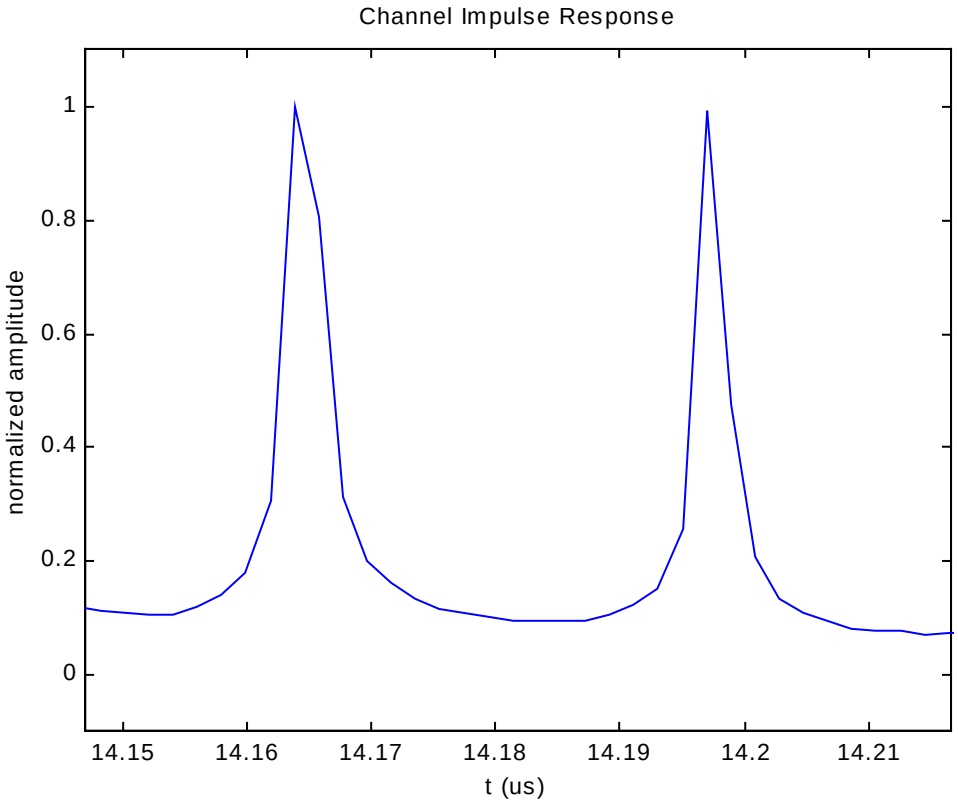

Figure 4.9: Channel Impulse Response based on the Two-Ray Model

4.6 Simulation of a Real Digital System

The next part of the research deals with simulating a real system with the channel models. The block diagram of both the transmitters and receivers are as shown below.

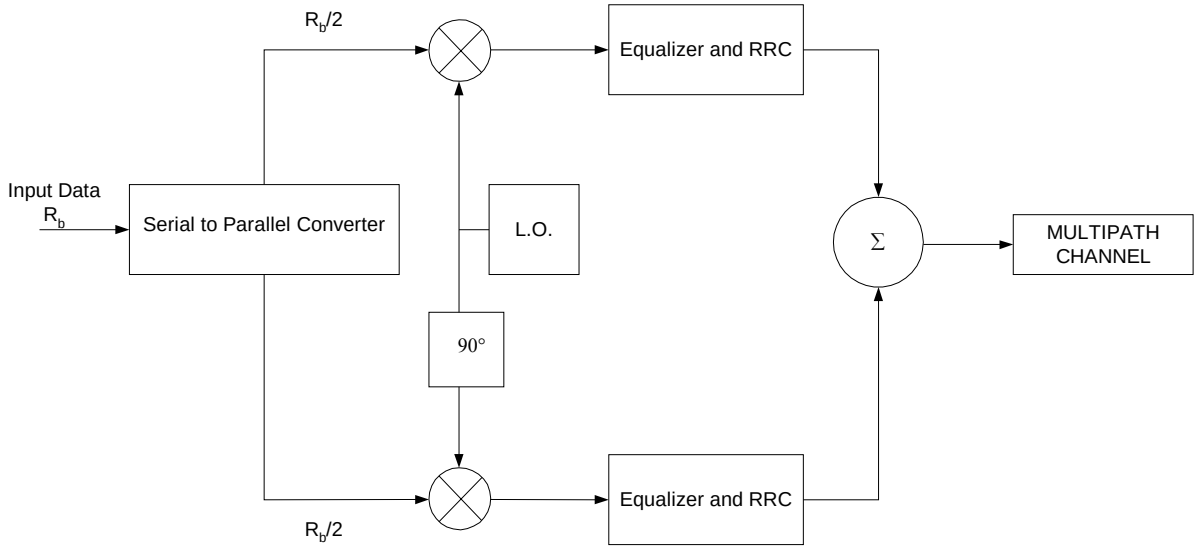

Figure 4.10: Block Diagram of the QPSK transmitter used in the simulation

The digital signal is first converted into two parallel bit streams that are orthogonal to one another, the in-phase and quadrature components. The signals are then sent through an equalizing filter and a root raised cosine (RRF) filter. These two filters are required to satisfy Nyquist's criterion for eliminating intersymbol interference (ISI). The signals are summed up before transmission.

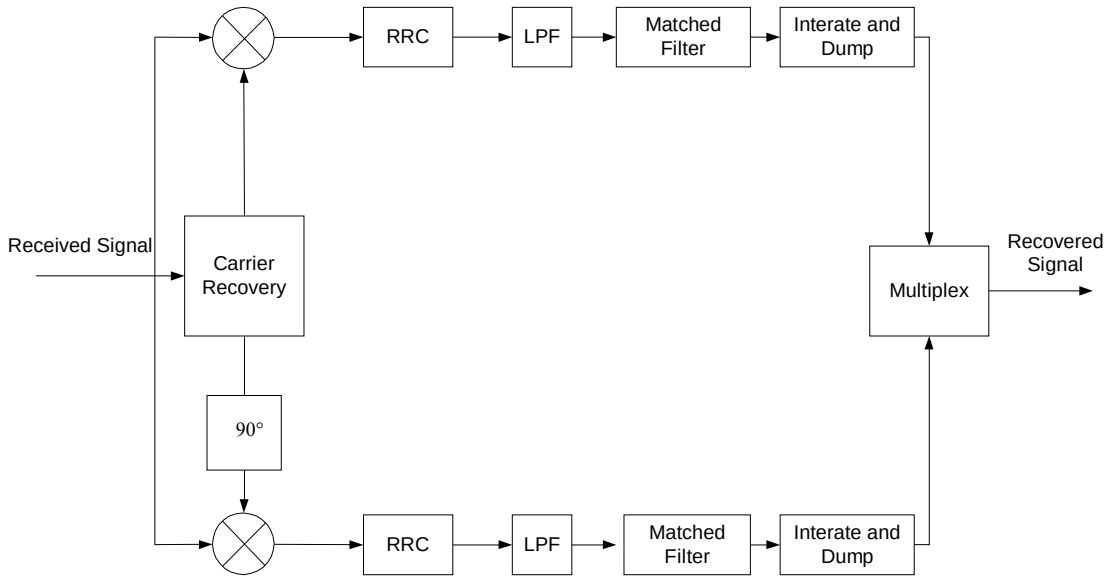

Figure 4.11: Block Diagram of the QPSK receiver used in the simulation.

At the receiving end, the QPSK signal is converted back to its in-phase and quadrature components. They are filtered by the RRC and low-pass filter before a matched filter. The matched filter is used to maximize the signal while minimizing the effects of noise. An integrate-and-dump process is applied to retrieve the digital binary signal. The two orthogonal binary signals are then multiplexed to form the recovered signal.

The channel models with varying lake level with respect to the mean sea level will be presented first. A simulated QPSK signal at a specific data rate will be sent through the three channel models that are investigated. Following that, eye patterns of the output will be shown. The eye patterns will show how the channel affects the performance of the system.

At any specific lake level, the bit error rate versus maximum transmissible data rate curve will be generated.

4.6.1 Channel Models

The following three plots describe the channel behavior for the various heights of the lake above mean sea level. We will investigate the maximum, mean, and minimum level of the lake with respect to the mean sea level. Note from the following three plots, that as the lake level is increased above mean sea level (AMSL), the coherence bandwidth of the system decreases. The unit used in the magnitude are in decibels.

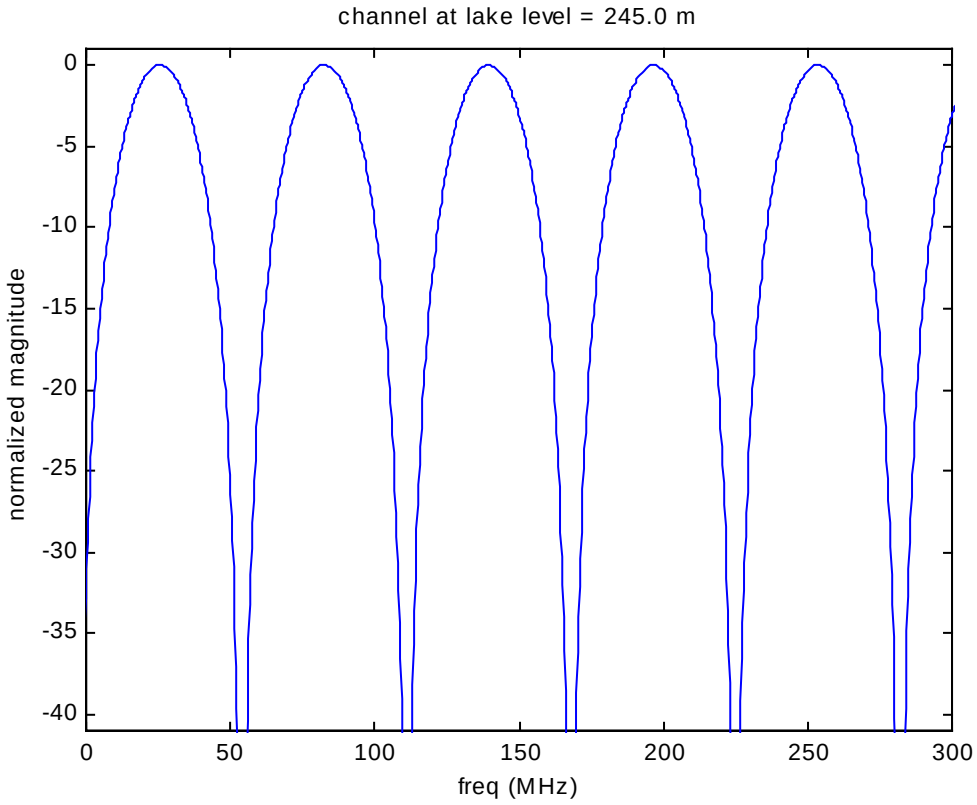

Figure 4.12: Channel model at 245.0 m AMSL

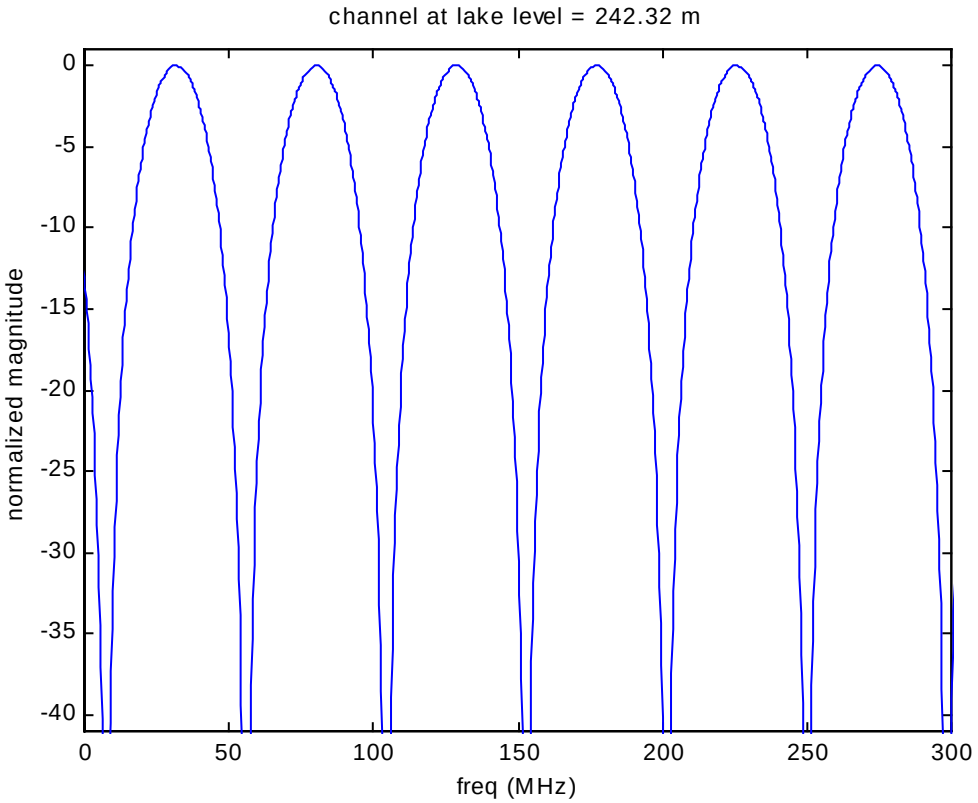

Figure 4.13: Channel model at 242.32 m AMSL

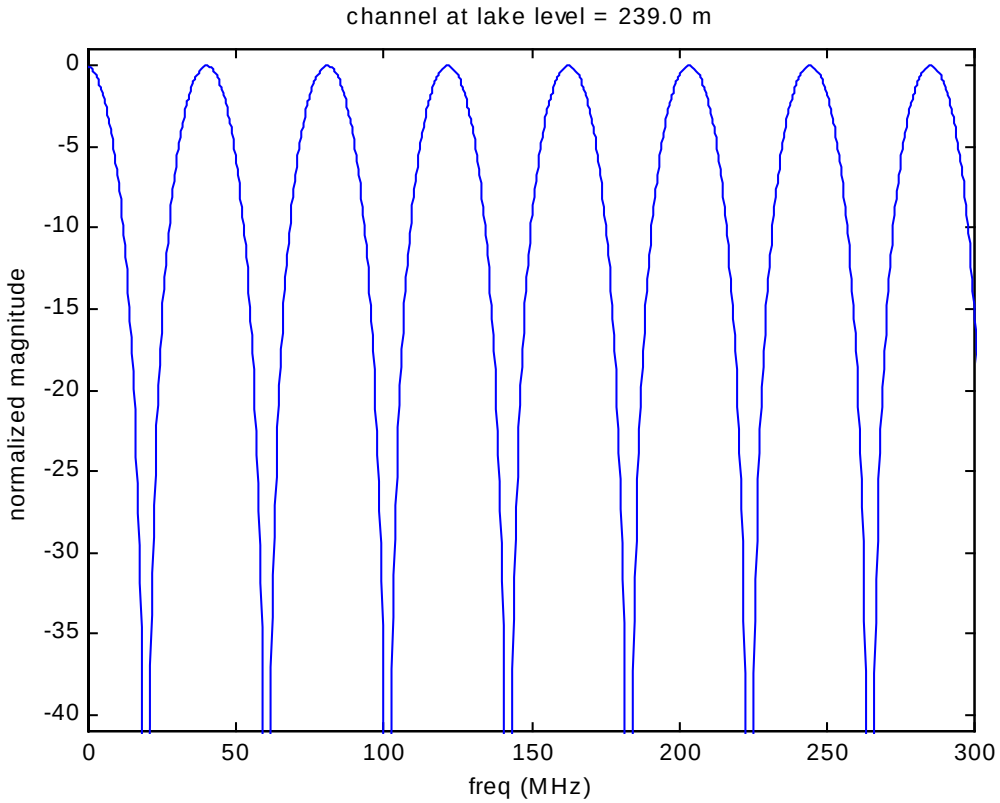

Figure 4.14: Channel model at 239.0 m AMSL

4.6.2 System Simulation with Data Rate of 40 Mbps and Varying Lake Levels.

The digital signal that will be used will be QPSK modulated. From Figure 4.8, both the in-phase and quadrature component of the signal will be sent through an equalizer and a root-raised cosine (RRC) filter at a roll-off factor, r. The RRC filter is used because a brick-wall filter is not realizable in the real world. The roll-off factor essentially increases the occupied bandwidth of the signal, and yet decays much faster than 1/x so that the clock jitter in the sampling times does not cause appreciable ISI [Cou97].

$$B_T = R_s\,(1 + r) \tag{4.5}$$

Equation 4.5 shows that in an ideal situation, where a simple brick-wall filter can be constructed (r = 0), the transmission bandwidth (B_T) will be equal to the symbol rate (R_S). However, when roll-off is introduced (r > 0), the transmission bandwidth will be higher than the symbol rate.

In this section, we will investigate a system with a bit rate of 40 Mbps with a roll-off factor of 0.25.

Figure 4.16 shows the simulation being carried out at the Intermediate Frequency (IF), since it will be too time consuming, and may not be possible, to run the system at the actual 28 GHz carrier frequency.

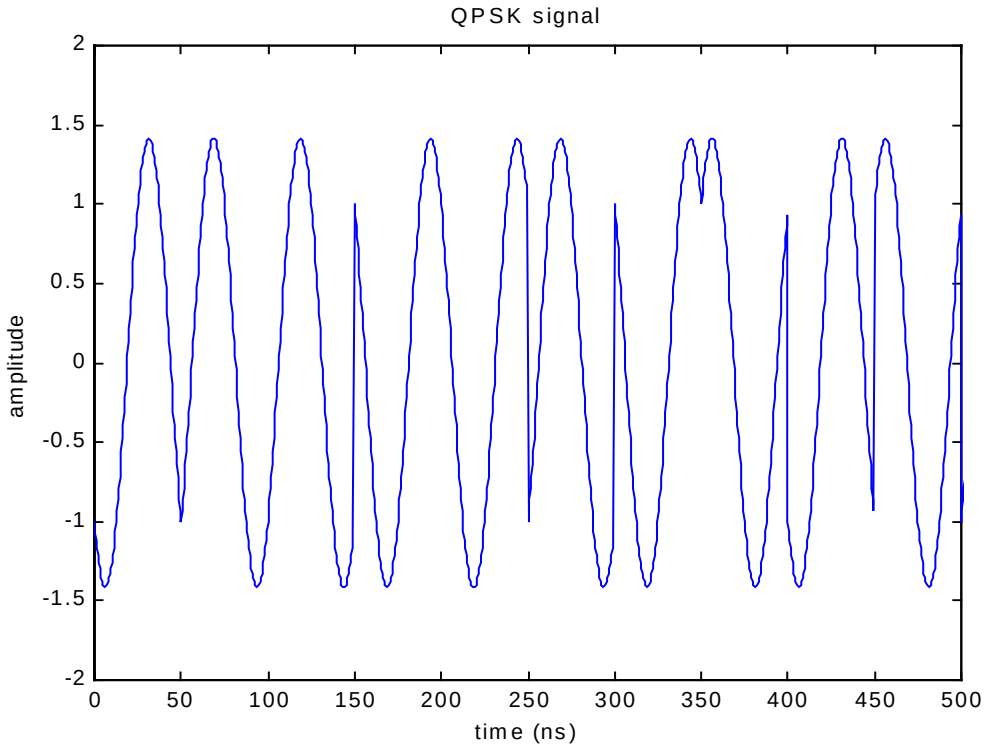

Figure 4.15: QPSK signal in time at the transmitter (unfiltered)

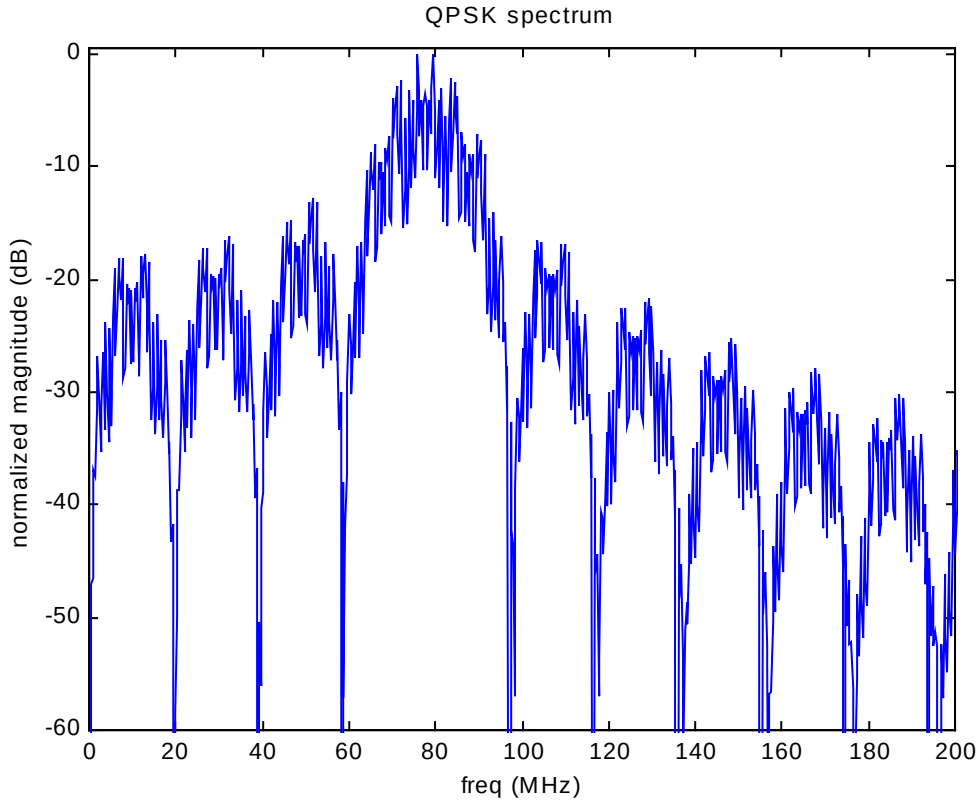

Figure 4.16: QPSK spectrum

The signal shown in the previous two figures will be sent through an equalizer and a RRC filter before being tested with the three channels as presented in Figures 4.12 through 4.14.

At the receiving end, the signals will again be filtered by the RRC filter, and then with a low-pass filter. The output from the low-pass filter is sent through a matched filter before an integrate-and-dump process is done to retrieve the original digital binary signal.

The three diagrams that follows shows the eye diagrams of the received signal through three different channels. The C/N ratio is kept constant throughout the simulation, and the observed effects are due to the fading channel, and not the system noise.

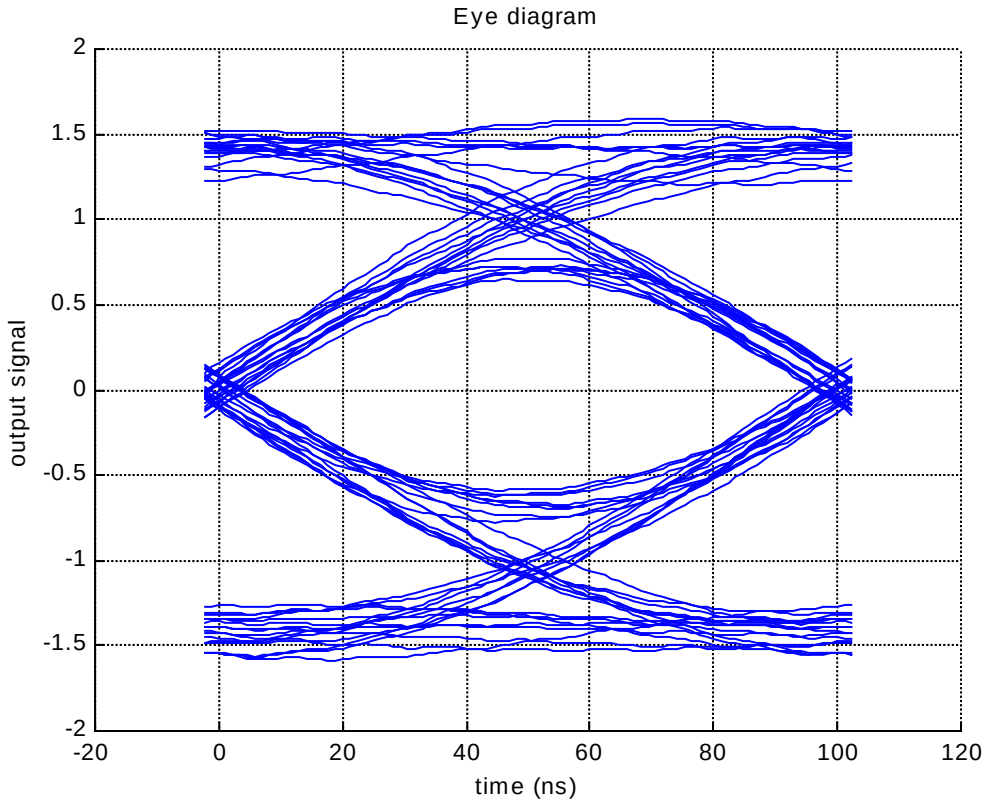

Figure 4.17: Eye Diagram of the output through channel with lake level = 245.0 m AMSL.

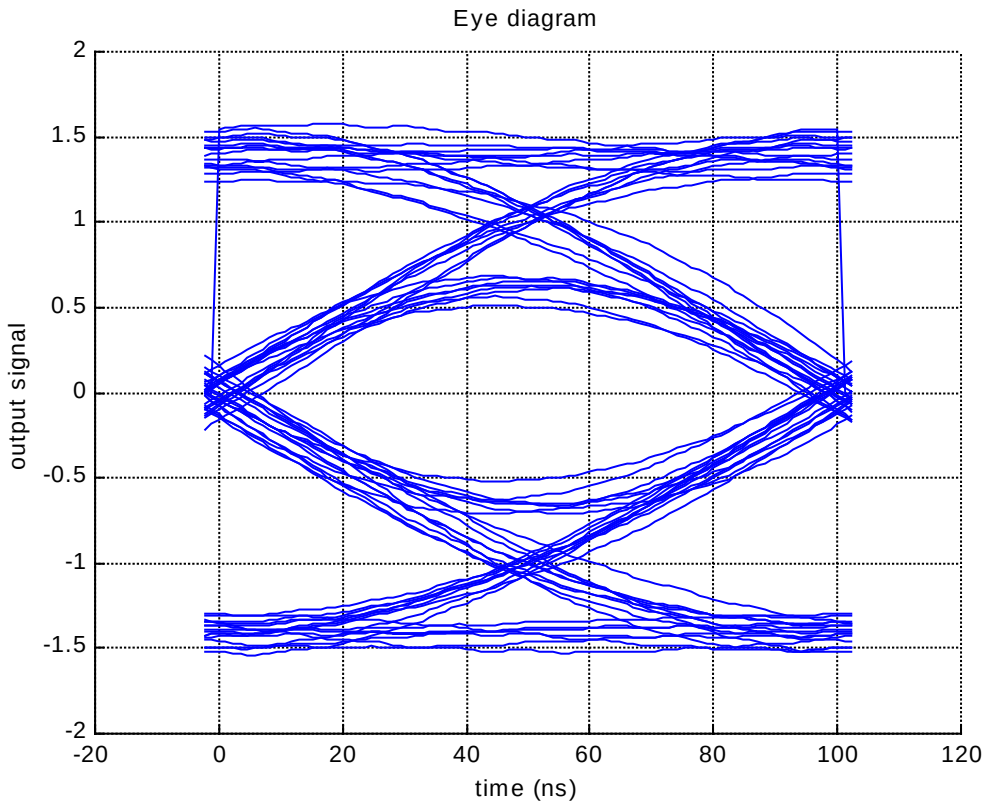

Figure 4.18: Eye Diagram of output through channel with lake level = 242.32 m AMSL.

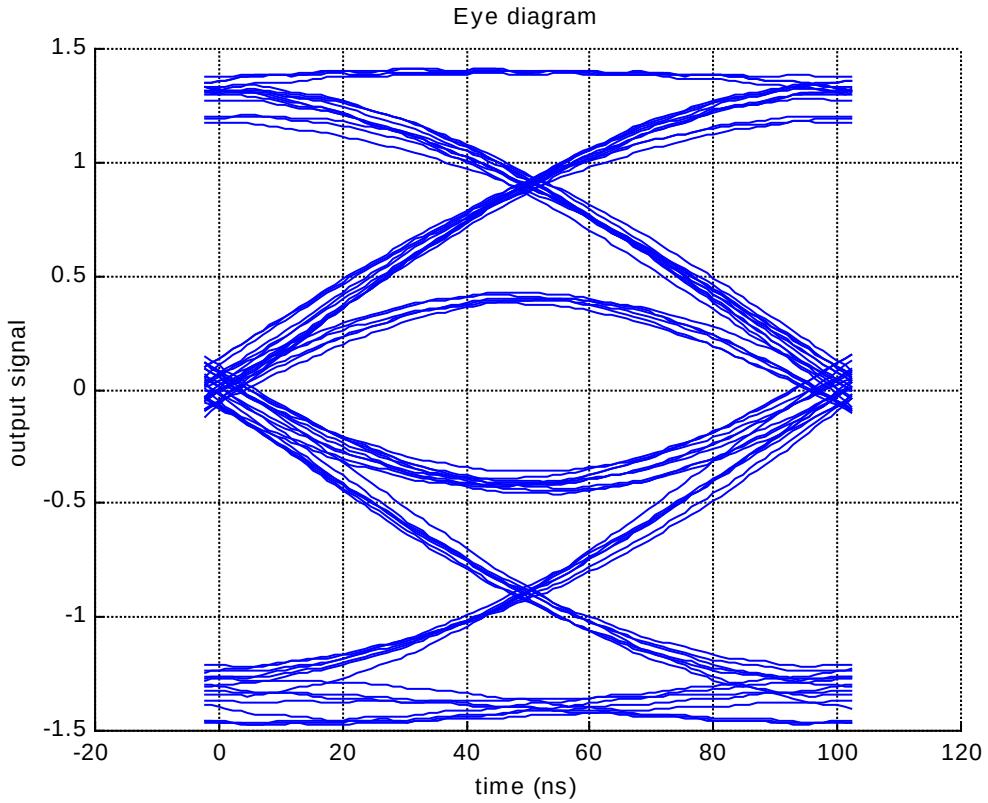

Figure 4.19: Eye Diagram of output through channel with lake level = 239.0 m AMSL.

Under normal operating conditions, the eye will remain open. This means that there are no detected bit errors. As the eyes start to close in, the RMS noise will increase, thus causing the bit errors to increase.

4.6.3 System Simulation with Lake Level of 245.0 m AMSL and Varying Data Rate

In this section, we will illustrate the performance of the system at a fixed lake level with varying data rate. A lake level of 245.0 m AMSL will be used, and the three data rate that will be investigated will be 40 Mbps, 60 Mbps, and 80 Mbps.

The eye diagrams that follow will allow us to compare the systems performance as the data rate is varied.

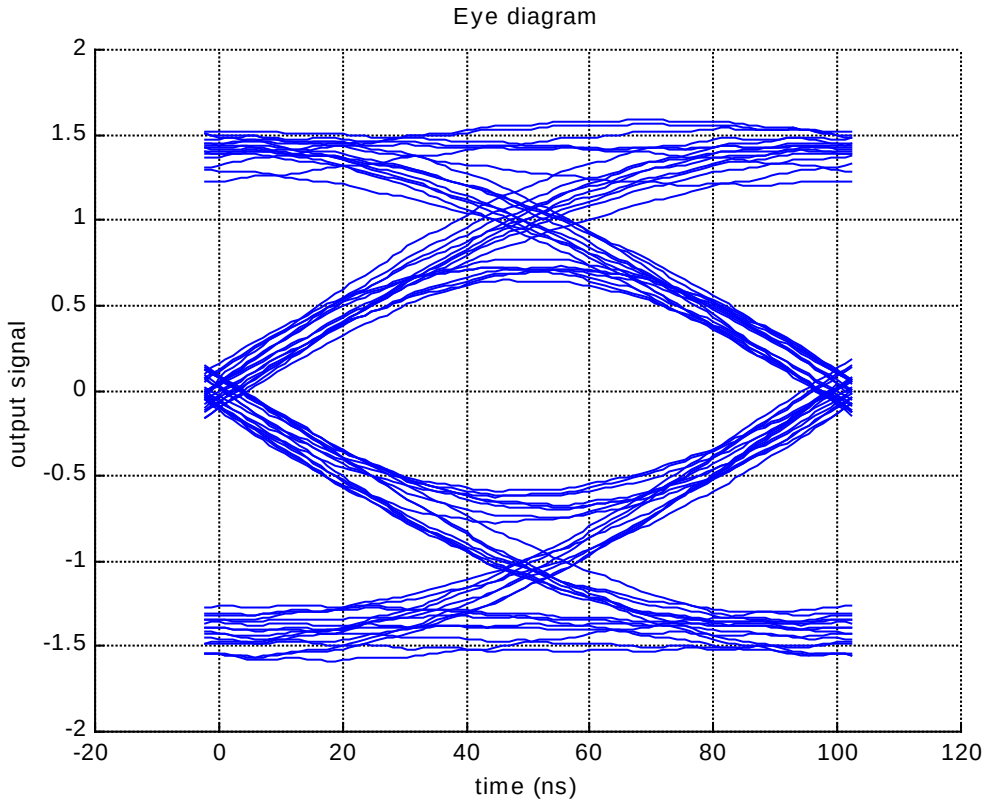

Figure 4.20: Eye Diagram of output with R_b = 40 Mbps

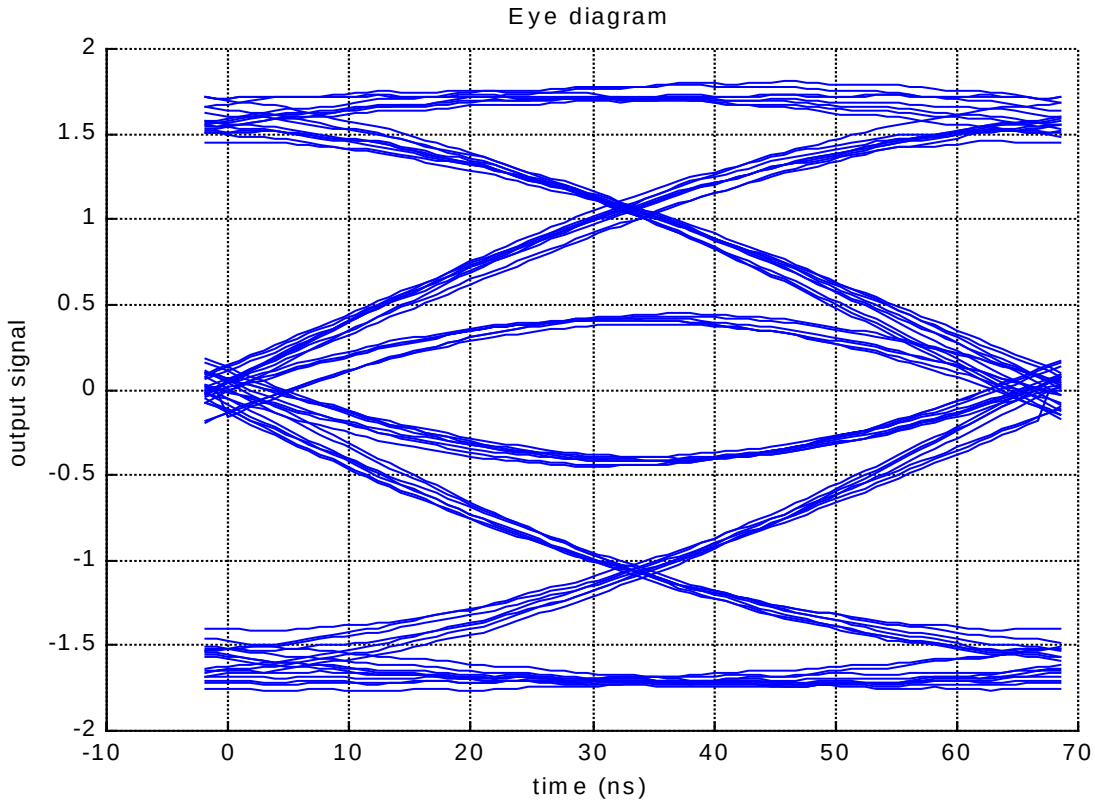

Figure 4.21: Eye Diagram of output with R_b = 60 Mbps

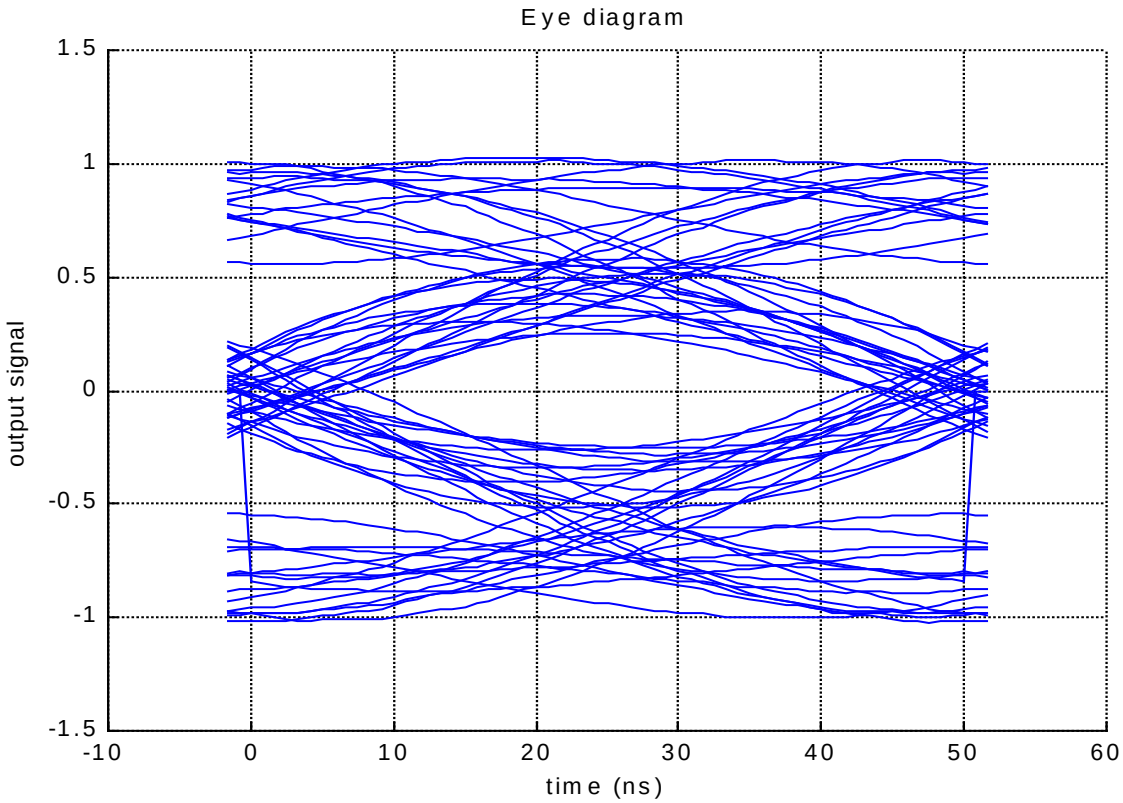

Figure 4.22: Eye Diagram of output with R_b = 80 Mbps

By comparing the three figures above, we can conclude that the eye diagram closes as the data rate of the system increases. The overall performance of the system is dependent on the fading channel characteristics, since the channel shifts throughout the day, and the signal might fall in the null region, causing an increase in errors. In the next section, the relationship between the BER and maximum transmissible data rate will be shown.

4.6.4 System Performance: The Relationship between BER and R_b

The dependence of the maximum transmissible bit rate and the BER can be described as follows. As the bit rate of a signal increases, the occupied bandwidth of the system increases. If the bandwidth of the signal exceeds the coherence bandwidth of the channel, part of the received signal will be attenuated.

In Section 4.6.2, the variation of the lake level causes the coherence bandwidth of the channel to change, as can be observed in Figures 4.17 through 4.19. The maximum transmissible data rate will change at different times of the day. By keeping the data rate constant and allowing the channel bandwidth to vary, we are able to see how the eye diagrams start to close, thus increasing the noise in the system.

Section 4.6.3 shows that at a specific lake level, when the bandwidth of the signal exceeds the coherence bandwidth of the channel, the system will break down. The eye diagrams of Figures 4.20 through 4.22 proves that an increase in the data rate of the system will increase the probability of the occurrence of errors.

The shifts that occur in the channel as the lake level changes will also affect the quality of the received signal. This is due to the location of the nulls in frequency. If the peak of the signal happens to fall on one of the nulls at a particular time in the day, the BER will increase.

Intuitively, as will be proven in the plots below, the system performance when the lake level is at 245.0 m AMSL fares better than when the lake level is at 239.0 m AMSL. This is to be expected, since the coherence bandwidth of the latter is less than that of the former.

The plots obtained below were done through the Monte Carlo method, and was averaged over the total bits that were run through the system.

Figure 4.23 shows the bit error rate performance of the system with the lake level at 245.0 m AMSL.

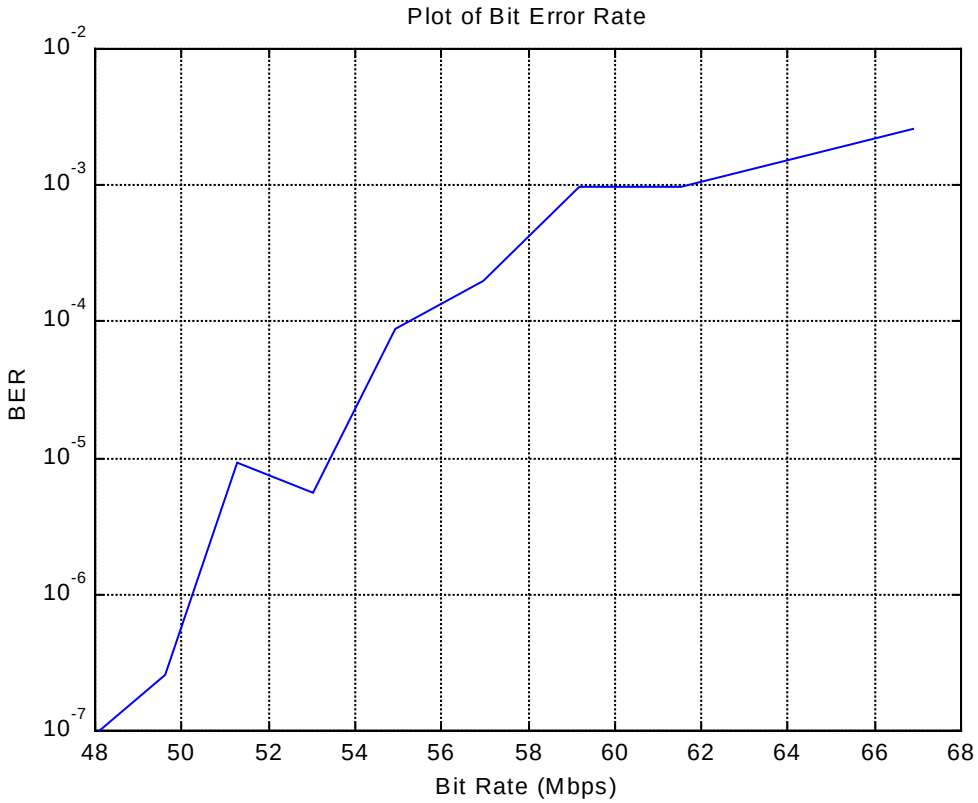

Figure 4.23: BER plot for channel with lake level = 245.0 m AMSL.

With the lake level at its maximum with respect to the mean sea level, the system starts to break down at about 51 Mbps.

Figure 4.24 shows the bit error rate performance of the system with the lake level at 242.32 m AMSL.

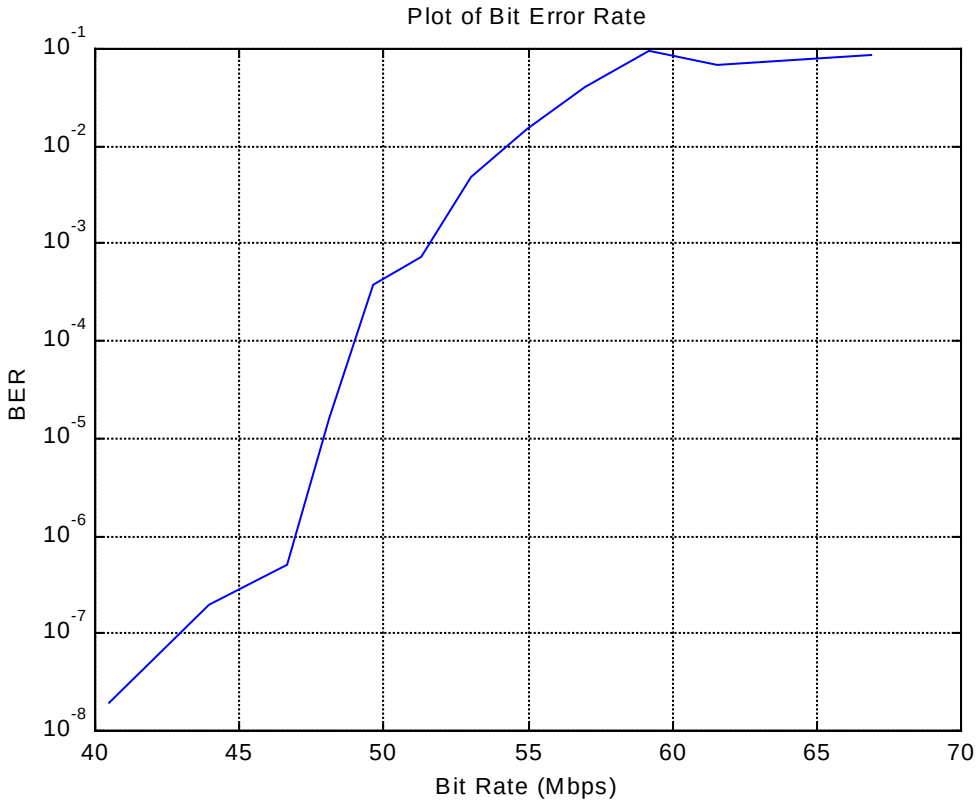

Figure 4.24: BER plot for channel with lake level = 242.32 m AMSL.

With the lake level at its mean with respect to the mean sea level, the system starts to break down at about 47 Mbps.

Figure 4.25 shows the bit error rate performance of the system with the lake level at 239.0 m AMSL.

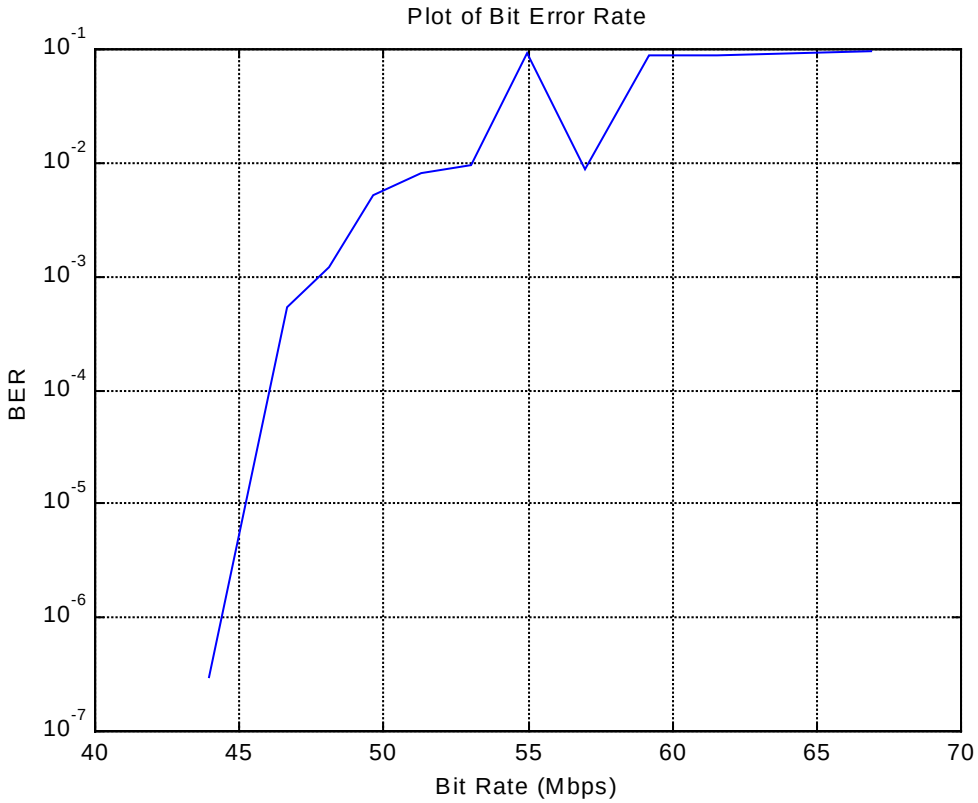

Figure 4.25: BER plot for channel with lake level = 239.0 m AMSL.

With the lake level at its minimum with respect to the mean sea level, the system starts to break down at about 44 Mbps.

Figure 4.26 below provides a side-by-side comparison among the three BER plots obtained.

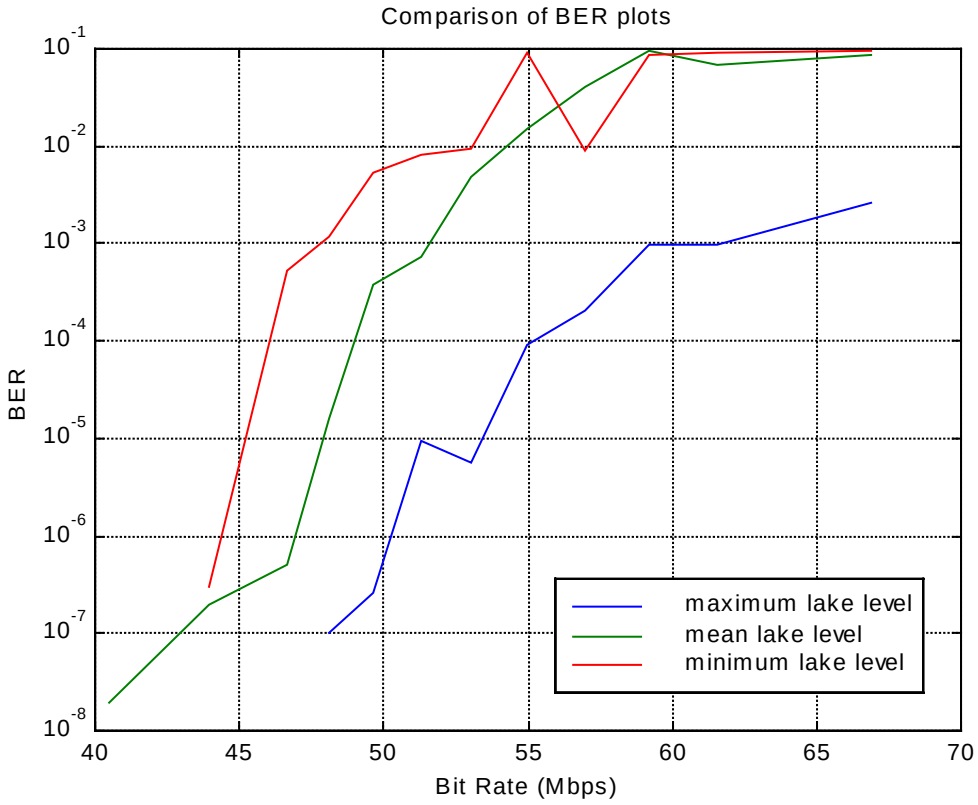

Figure 4.26: Comparison of BER plots for the three lake levels.

By comparison, when the lake level is at its maximum with respect to the mean sea level, it can be noted that the highest data rate is transmissible, while the minimum lake level with respect to the mean sea level has the lowest data rate based on the same BER requirements.

This agrees with the expected results, that is, as the coherence bandwidth of the channel increases, the better the performance of the communication link. Therefore, an LMDS

link at Smith Mountain Lake can be set up without too much degradation if the data rate of the system remains at about 45 Mbps.

Chapter 5
Analysis of Results and Future Work

The simulation results that were presented in the last chapter assume that the reflecting surface is smooth with specular reflection. This is the worst case scenario when the water is at its calmest.

In this section, we will discuss the effects of a rough surface, which is a more practical way of looking at the system.

5.1 Rough Surface Assumption

According to the Rayleigh Criterion as described in Equation 2.9, one method used to note whether or not the surface irregularities affect the diffusion of the reflected signal is to calculate the value of the standard deviation relative to the mean height.

Based on Equation 2.9, the reflected component will have an effect on the received signal when C is between 0.1 and 10. If C is less than 0.1, 100% reflection occurs and deep nulls will take place. This causes the received power to fluctuate as shown in Figure 4.3. If C is greater than 10, the reflected component is so diffused that it can be neglected

altogether. The received power will then have lower amplitudes, but the nulls that appear in Figure 4.3 may disappear.

Figure 2.8 provides an idea as to how the coherent power and incoherent power behave. When there is total reflection, all that will be seen at the receiver will be the coherent power. When the reflected power is scattered in all directions, the incoherent power will dominate. Since the incoherent power spreads over a large area, it carries no significant information. Therefore, it is basically noise that distorts the received (coherent) power.

From the derivation of the system model in Chapters 2 and 3, we are able to conclude that the angle of reflection - or grazing angle, α, is about 5°, remaining almost constant throughout the simulation. The variation of the lake level would not alter the grazing angle too significantly. This is because of the large distance between the transmitter and receiver (over 4 km), causing the angle to be 'flat'.

Based on

$$C = \frac{4\pi\sigma \sin\alpha}{\lambda} ,$$

the following equation can be derived through algebraic manipulations:

$$\sigma = \frac{C\lambda \sin\alpha}{4\pi} . \qquad (5.1)$$

To have specular reflection, the value of the root mean square (RMS) wave height, σ, has to be less than 1mm (0.04 in) high. If the reflected component were to be completely neglected, σ has to be greater than approximately 10 cm (0.32 ft). The latter condition may happen when there is heavy rain or strong wind. This means that the channel can be assumed to be flat and there will be no fading problems for the transmitted signal.

On the other hand, if the water surface remains relatively calm and the surface irregularities stay within 10 cm, the results shown in Chapter 4 provide a sufficient concept as to what we would expect to observe if a field measurement campaign were to be conducted.

At this point, there is not enough information available to conclude what could be expected of the received power as the waves propagate over the lake. Most of the studies on surface waves and fluxes were done over a wide and open ocean surface. The data collected from these studies will not be a valid assumption for a lake surface because the latter is significantly smaller and much more enclosed. A light breeze blowing over a deep ocean surface for a long period can cause waves of unimaginable height over time.

The following table, compiled by Pierson [Gee90], gives the reader some idea about the probable wave height that we would expect to see in an open sea. It has to be mentioned that for an enclosed lake, much like Smith Mountain Lake, the wave heights will be smaller and the waves steeper.

Table 5.1: Scale of Wind Force [Gee90].

Mean Wind Speed (knots)	*Descriptive Terms*	*Appearance of the Sea*	*RMS Wave Height (m)*
0	Calm	Sea like a mirror	0
2	Light air	Ripples with the appearance of scales are formed, but without foam crests	0.1905
5	Lights breeze	Small wavelets, still short but more pronounced: crests have a glassy appearance and do not break.	0.0381
9	Gentle breeze	Large wavelets; crests begin to break. Foam of glassy appearance	0.1524
13	Moderate	Small waves, becoming longer.	0.2667
19	Fresh breeze	Moderate waves, taking a more pronounced long form. Chance of some spray.	0.4572
24	Strong breeze	Large waves begin to form. The white foam crests are more extensive everywhere. Probably some spray.	0.7239
30	Near gale	Sea heaps up and white foam from breaking waves begins to be blown in streaks along the direction of the wind.	1.0287
37	Gale	Moderately high waves of greater length. Edges of crests begin to break into spindrift. The foam is blown in well marked streaks along the direction of the wind.	1.3716
44	Strong gale	High waves; dense streaks of foam along the direction of the wind. Crests begin to topple, tumble, and roll over. Spray may affect visibility.	1.7526
52	Storm	Very high waves with long overhanging crests. The resulting foam, in great patches, is blown in dense white streaks along the direction of the wind. On the whole, the surface of the sea takes on a white appearance. The tumble of the sea becomes heavy and shock-like. Visibility affected.	2.2098
60	Violet storm	Exceptionally high waves. The sea is completely covered with long white patches of foam lying along the direction of the wind. Everywhere the edges of the rests are blown into froth. Visibility affected.	2.8194
68	Hurricane	The air is filled with foam and spray. Visibility very seriously affected.	3.429

5.2 What the Results Mean to an LMDS Link

So far, the results that have been shown prove that the coherent bandwidth plays a crucial role in the radio link as the LMDS waves propagate over water.

As stated in Section 5.1, as long as the standard deviation of the surface irregularities stays within 10 cm of the mean height, the reflected component will cause the nulls to occur in the channel and a degradation of the performance of the system will occur. This can be observed in the plots of Chapter 4. A maximum data rate of approximately 45 Mbps can be transmitted if QPSK was used in the modulation. Ironically, the system performance will improve as the roughness of the water surface increases, albeit the signal will be weaker. However, for most applications, the maximum data rate of 45 Mbps is still sufficient to handle most voice and video applications without degrading the performance.

5.3 How to Begin a Field Measurement Campaign

The measurements which were carried out in [Man99] were done for low data rate transmissions at LMDS frequencies. A great deal of available commercial equipment, especially the digital signal generators and vector signal analyzers, would have a maximum data rate of approximately 20 Msymbols/s. The measurements that we need to perform will far exceed the data rate available. The main reason for this shortcoming is because commercial equipment caters mainly to the mobile wireless test beds such as CDMA, or W-CDMA, and TDMA. The data rate requirements for these systems are not as high as fixed broadband wireless access. Moreover, commercial equipment that is available could cost anywhere from $50,000 to $100,000.

To overcome this shortcoming, we propose to build some blocks in the system. Commercially available LMDS modems and upconverters can be used to generate high data rates that can serve our research purposes.

5.3.1 Measuring the Wave Level and Wind Speed

Measurements on wave levels and wind speeds are usually done for a wide open sea where radar backscattering is important. For our application, there is not much available data to back the simulated and measured results.

In order to collect a reasonable amount of data that we can use, we will need to employ the use of a wave pole to measure the height of the waves over a period of time with a wind sensor facing in the direction of the wind. This will allow us to draw a conclusion about the relationship between wave height and wind speed. The information will be crucial to the received power and performance of the LMDS link.

5.3.2 Measuring the LMDS Link Performance

The amount of time and money that are allocated for this research project determines the kinds of equipment that can be used for the measurements.

Figure 5.1 below shows the block diagram of a potential configuration that could be used.

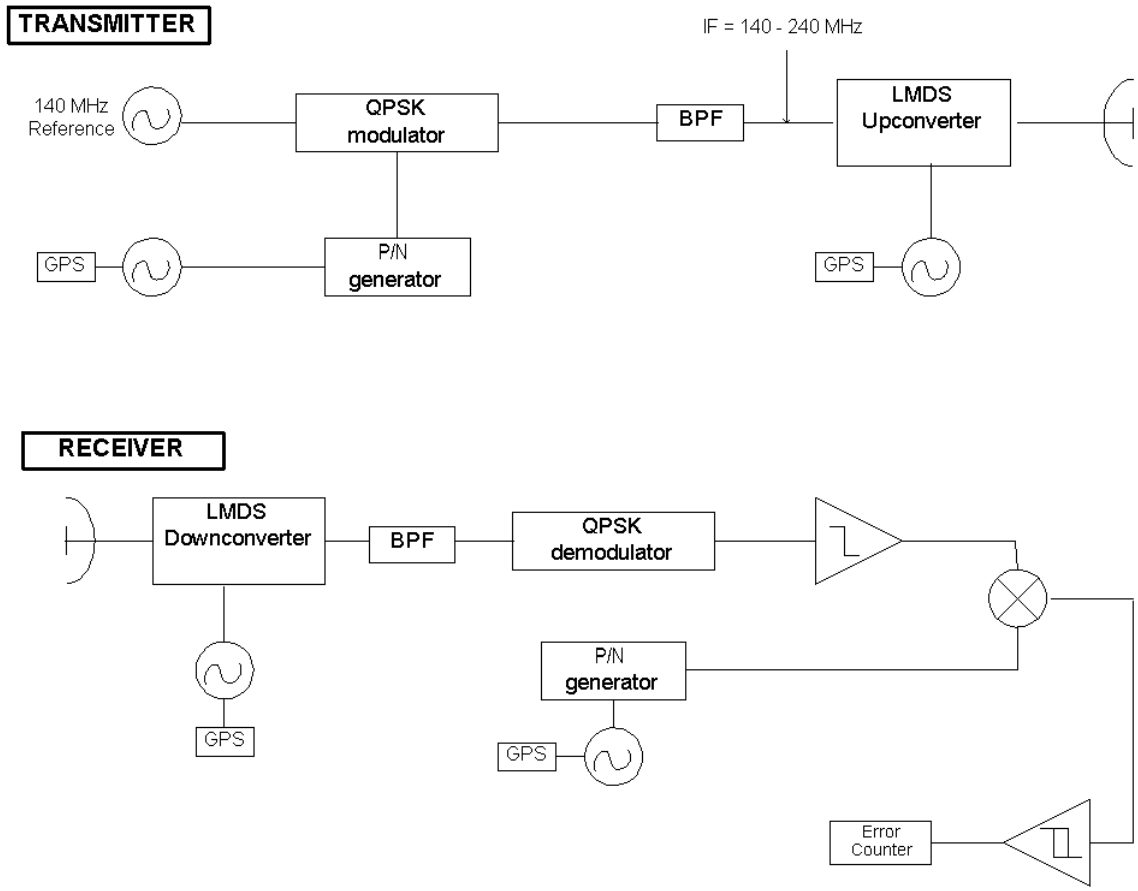

Figure 5.1: Block diagram of a possible hardware configuration for field testing

5.3.2.1 The Transmitter

The QPSK generator will be nothing more than two double-balanced mixers, with a 140 MHz oscillator connected to it as a reference. A Pseudorandom-Noise (PN) generator will be used to determine the data rate of the transmission. In the block diagram above, we showed a 60 MHz clock, which translates to a 120 Mbps data rate.

A bandpass filter (BPF) will have to be built depending on the specifications of the hardware. LMDS up/down converters are readily available in the market. A frequency band of 100 MHz for the filter should be more than sufficient for the purposes of this

research. The local oscillator (LO), at the LMDS up-converter, and the PN generator clock will be connected to a Global Positioning Device (GPS). This will be used for synchronization purposes and to determine the delay times. An example of the up-converter can be found at [Man99], where the author used an mm-Tech Model TRSS001 Solid State Transmitter. This device is capable of translating the signal to 27.500 – 27.537 GHz. It also has a 30 dB gain.

5.3.2.2 The Receiver

After receiving the signal at the antenna, it will be downverted with an LMDS down-converter. There are many manufacturers who produce the equipment. As in the upconverter, mm-Tech's RVSS001 Ka-band can be used for this purpose [Man99]. A data slicer will be used to translate the received signal into an analog version of the PN sequence. This output will be multiplied with the original PN sequence and a Schmitt Trigger will be used to determine the error that would have occurred at the output. Since the two sequences should be equal, an error will be detected whenever the multiplication produces a 'low' output.

An easier alternative is to use a loop-back configuration. This simply means that the received signal will be retransmitted back to the transmitter. If the data is taken over a long time period and averaged over several days, the height factor of the transmitter and receiver could be ignored.

Since we do not know the phase behavior and how it would affect the results at this point, it is fair to assume that the phase remains static in the initial measurement. If the phase becomes a problem, it can be easily tracked with a Johnson counter. This counter, due to its 4-bit (modulo-8) nature, will have to operate at four times the rate of transmission.

5.3.3 Channel Characterization

The unpredictability of the channel can be solved by employing the use of an ultra wideband (UWB) channel sounder currently developed in the CWT laboratory. The idea of a channel sounder is to create a power profile of the channel. Information that can be extracted from a channel sounder includes the mean excess delay, RMS delay spread, and coherence bandwidth. The data collected from the channel sounder can be compared with both the simulated and measured results.

The ability to characterize the large spectrum available at the LMDS frequency range will allow researchers to further investigate the optimum modulation scheme and data rate that can be used in any system.

Chapter 6
Conclusion

By assuming that all the reflected power is seen by the receiver, we have provided the reader with the worst-case possible scenario in which we can propagate LMDS waves over-water. We know that a maximum value of about 45 Mbps can be transmitted without any severe degradation to the received signal.

The nulls that occur is due to the total reflection of the multipath component. This creates a coherence bandwidth that limits the data rate of the system.

From the simulation, we concluded that a maximum data rate of 45 Mbps can be sent through the link without significant degradation of the signal. This may cause a problem with the second generation LMDS equipment, where the LMDS hubs are able to transmit information at OC-3 (155 Mbps) or higher.

Due to the unpredictability of the time-varying surface roughness of the lake, it is extremely difficult to anticipate what we would expect from propagating millimeter waves over a lake surface. Brown [Gee90] showed that it is tremendously tedious to calculate the amount of incoherent power that actually arrives at the receiver. Oceanographers usually draw conclusions of the channel behavior over an open sea surface by collecting data over a long period of time. One very crude way to model the effects of scattering is to use another ray with the reflection coefficient of less than unity.

This very reason prompted us to device method of measuring the performance of the system that includes not only the hardware necessary to measure the signal strength and error calculations, but a simple, yet effective, way to characterize the randomness of the lake surface. With the development of a UWB channel sounder, it makes it extremely easy for researchers to study the channel characteristics and make available different adaptive antenna array types to capture most of the coherent power that arrives at the receiver.

BIBLIOGRAPHY

[All89] J.E. Allnutt, *Satellite-to-Ground Radiowave Propagation*, London, England: Peter Peregrinus Ltd., 1989.

[And98] O. Andrisano, et.al., *Millimeter Waves for Short-Range Multimedia Communication Systems*, Proceedings of the IEEE, Vol. 86, No. 7, July 1998.

[Bec63] P. Beckmann, A. Spizzichino, *The Scattering of Electromagnetic Waves from Rough Surfaces*, Oxford, England: Pergamon Press Ltd., 1963.

[Bel82] Members of the Technical Staff, Bell Telephone Laboratories, *Transmission Systems for Communications*, n.p., 1982.

[Col85] R. Collin, *Antennas and Radiowave Propagation*, New York: McGraw Hill, 1985.

[Cou97] L.W. Couch, *Digital and Analog Communication Systems*, 5th Edition, New Jersey: Prentice Hall, 1997.

[Gee90] "G. Geernaert and W. Plant, Eds.," *Surface Waves and Fluxe:, Volumes I and II*, Dordrecht, The Netherlands: Kluwer Academic Publishers, 1990.

[Klo97] C. Kloch, J.B. Andersen, Radiosity – *An Approach to Determine the Effect of Rough Surface Scattering in Mobile Scenarios*, Antennas and Propagation Society International Symposium, 1997. IEEE, 1997 Digest.

[Man99] E. Manning, *An Introduction to Local Multipoint Distribution Services with an Investigation into the Effects of Vegetation on the Radio Channel*, M.S. Thesis, ECPE Department, Virginia Tech, Blacksburg, VA, 1999.

[Nar96] R. Narayanan, et.al., *Millimeter Wave Specular and Diffuse Multipath Components of Terrain*, IEEE Transactions on Antennas and Propagation, Vol. 44, No. 5, May 1996.

[Par94] J.D. Parsons, *The Mobile Radio Propagation Channel*, New York: John Wiley and Sons, 1992.

[Rad00] "Introduction: Radiant Networks PLC", [Online document], [2001 Mar. 3], Available at HTTP: http://www.radiantnetworks.com

[Rap99] T.S. Rappaport, *Wireless Communications Principles and Practice*, New Jersey: Prentice Hall, 1999.

[Roa01] "Smith Mountain Lake", [Online document], [2001 Mar.14], Available at HTTP: http://www.roanoke.com/smithmountainlake

VITA

Chin Khee Tan began his graduate studies with the Bradley Electrical and Computer Engineering Department (ECPE) at Virginia Tech in the fall of 1999, after graduating from Michigan Tech in 1998.

He was offered a full Graduate Teaching Assistantship (GTA) upon joining Virginia Tech. His responsibilities as a GTA include grading homework assignments and exams in addition to providing tutorial sessions and office hours in the Signals and Systems courses.

Mr. Tan joined the Center for Wireless Telecommunications (CWT) as a Graduate Research Assistant (GRA) beginning in the summer of 2000 where he had the opportunity to work with Dr. Charles Bostian and most of the other faculty and student researchers in the center. His initial responsibilities were to oversee and maintain the LMDS network at Virginia Tech, working closely with the Communication Network Services (CNS), before embarking on his research thesis on the feasibility of setting up a fixed broadband wireless access over a lake surface.

His research interest encompasses most wireless telecommunications applications, including cellular communications and fixed broadband wireless access.